Numerical Modelling of Granular Beds in Rotary Kilns

M. A. Romero Valle

Master of Science Thesis

TU Delft Delft University of Technology

Department of Applied Mathematical Analysis

Numerical Modelling of Granular Beds in Rotary Kilns

Master of Science Thesis

For the degree of Master of Science in Computer Simulations for Science and Engineering at Delft University of Technology

M. A. Romero Valle

September 16, 2012

Faculty of Electrical Engineering, Mathematics and Computer Science · Delft University of Technology

Delft University of Technology
Department of
Faculty Electrical Engineering, Mathematics and Computer Science
(EEMCS)

The undersigned hereby certify that they have read and recommend to the Faculty of Electrical Engineering, Mathematics and Computer Science for acceptance a thesis entitled

Numerical Modelling of Granular Beds in Rotary Kilns

by

M. A. Romero Valle

in partial fulfillment of the requirements for the degree of

Master of Science Computer Simulations for Science and Engineering

Dated: September 16, 2012

Supervisor(s):

Dr. D.J.P. Lahaye

Reader(s):

Prof. Dr. Ir. K. Vuik

Dr. Ir. W.T. van Horssen

Dr. Ir. S. van Zuijlen

Ir. R. Sadi

Abstract

In process engineering applications numerical models are needed to make extensive analysis for the design and operation of unit operations. In the present work, a transversal granular flow model and two numerical models for the description of the granular bed of a rotary kiln are developed for the analysis of a Calcium Aluminate rotary kiln from an industrial partner.

From the transversal granular flow model it is concluded that the kiln from the industrial partner is probably not in a rolling mode. This hints the possibility that there is a non-optimised mixing in the kiln which could bring adverse consequences in the production and current modelling approaches of the studied rotary kiln.

A validated one-dimensional rotary kiln model is developed taking into account different approaches found in the literature. Simplified sintering reaction kinetics are proposed by considering experimental X-Ray Diffraction data. The one-dimensional model is successfully used to describe the properties of the product when changing air to gas ratio of the combusting gases in the kiln from the industrial partner.

Furthermore, a two-dimensional transversal model for granular bed heat transfer is developed to explore whether a full granular flow model is necessary in order to have a sufficiently accurate description of the granular material properties of the kiln from industrial partner. It is concluded that due to the low loading of the analysed CAC kiln, a one-dimensional model is sufficient to make a sensitivity analysis on the operating conditions and design variables of the kiln if the bed has a rolling mode with a active layer of 5% to 20% of the bed height.

Further research must be done in order to characterise the transversal flow of the analysed kiln in order to develop more complex kiln models.

Table of Contents

List of Figures

Acknowledgements

First of all, I would like to thank my supervisor Dr. D.J.P. Lahaye for his assistance during the writing of this thesis, Prof. Dr. R. Nabben and Prof. Dr. Ir. K. Vuik for their support as COSSE coordinators, Dr. Eng. L. Portela for his support concerning multiphase flow, Dr. D. Van Puyvelde for his patience and expertise with granular flow and industrial applications, and Ir. Rudy Sadi for his expertise in operational and practical aspects of the kiln.

I appreciate the support from my friends from Germany and The Netherlands, without them my life would have been extremely boring. Very special thanks to my friends from Mexico which also contributed with support at all times.

I thank my family for their support, which even consisted in the discussion of possible modelling approaches and the future of Chemical Engineering. Most importantly, I thank my future wife Paola for her love and support throughout the writing of this thesis.

I express my gratitude to the European Union Commission for funding my Master of Science studies through an Erasmus-Mundus Scholarship.

Delft, University of Technology
September 16, 2012

M. A. Romero Valle

"Good things come to those who work their butts off and never give up."
— *Unknown Author*

Chapter 1

Introduction

1-1 Rotary Kilns

The main motivation for the present thesis is to give insight into the phenomena that occur inside a Calcium Aluminate Cement (CAC) kiln in order to make its operation more efficient.

The present project deals with the consequences the kiln granular material bed has due to changes in kiln operating conditions and its design. The aim is develop an aid to facilitate the design and operation of CAC kilns.

Rotary kilns are employed to carry out a wide range of operations such as the reduction of oxide ore, the reclamation of hydrated lime, the calcination of petroleum coke and the reclamation of hazardous waste. However, they are much more widely known for their place in the cement industry as the main stage for the manufacture of cement.

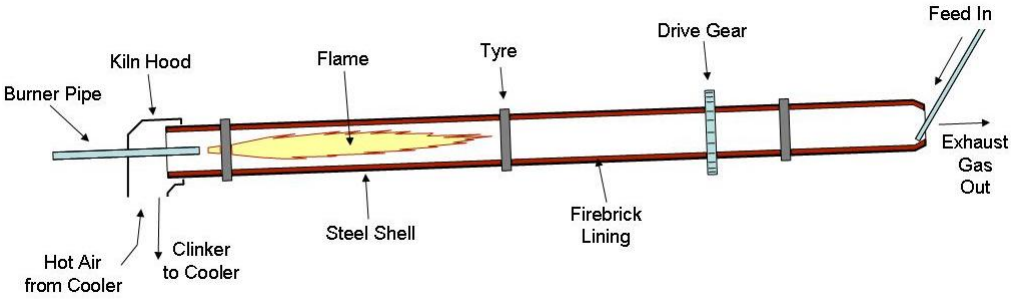

Figure 1-1: Cement Kiln

A rotary kiln is a pyro-processing device used to raise materials to high temperatures. It is a long horizontal cylinder with a certain inclination with respect to its axis. Material within the kiln is heated to high temperatures so that chemical reactions can take place. A rotary kiln is therefore fundamentally a heat exchanger from which energy from a hot gas phase is transferred to the bed material [6].

There are several configurations for rotary kilns. The rotary kiln in question [39] is a counter-current gas direct fired Calcium Aluminate Cement rotary kiln.

As it can be observed in Figure 1-1, a rotary kiln is a long, narrow cylinder. It commonly is inclined 2 to 5 degrees to the horizontal rotating at 0.25 to 5 rpm. The length/diameter is usually within the range from 10 to 35 m, depending on the residence time needed [38].

Rotary kilns can also be considered as solid-solid chemical reactors, in which one has mainly heat transfer interactions with a gas phase. The phenomena in the solids phase will be addressed with a certain level of detail as it will be the focus of the present project.

1-1-1 Kiln Fill Geometry

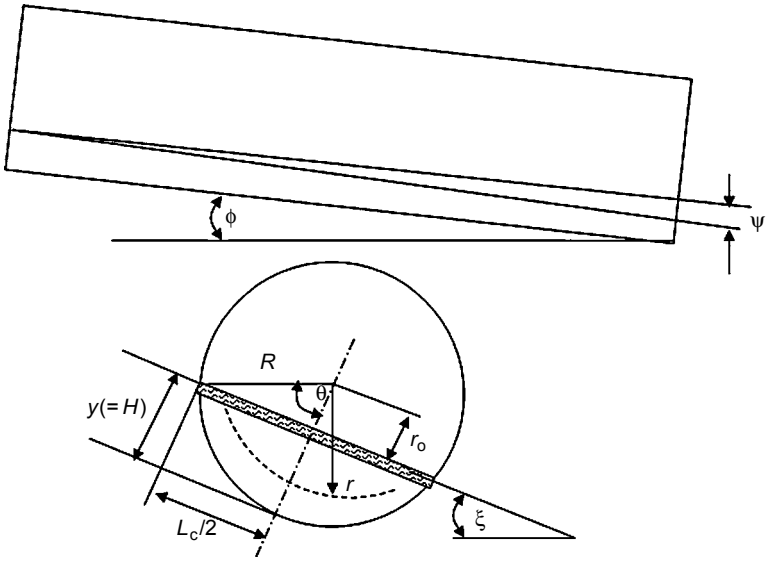

Figure 1-2: Kiln fill geometry [6]

The definition of kiln load is the percentage of cross sectional area of the cylinder occupied by the granular material. Boateng [6] also mentions that one can make a distinction between a lightly and a heavily loaded kiln. This is due to the fact that there are different theoretical and empirical models for the residence time, volumetric flow and velocity profiles of the axial component of the flow of particles in the kiln. The industrial kiln in question is a lightly loaded kiln. This means that the degree of fill can be taken constant within the length of the kiln, in other words, in Figure 1-2, $\Psi \approx 0$ [6]. Ψ represents the angle between the surface of the bed material and kiln axis.

1-2 Calcium Aluminate Cement Production

The rotary kiln to be modelled is not a typical Portland Cement kiln, thus it has different chemical reactions and operating conditions to most of what is presented in literature. In fact, it is a Calcium Aluminate Cement kiln.

The main difference between the described kiln from Portland Cement Kilns is that there is no calcination reaction, only the sintering of Alumina and Lime takes place. In Section 1-6 a short overview on the sintering chemical reactions taking place in the studied kiln will be given

1-3 Previous Modelling Approaches

There are various approaches in the literature for the modelling of a rotary kiln. However, all of them make the distinction between two particular phenomena in the kiln, the freeboard part which consists of the combusting gases phase, and the granular bed.

Most of the approaches presented in literature deal with a CFD approach for the freeboard and a model for the granular bed which deals with chemical reactions and heat exchange [31, 6, 19, 46, 32, 35, 48, 22].

One then can divide the model into two different parts based on this observation:

- Freeboard CFD Model: work done by M. Pisaroni [39];
- Granular Bed Model: focus of the present project.

The simulation of the granular material bed usually uses input data from the freeboard simulation in a coupled or uncoupled way, depending on the influence of exothermic or endothermic chemical reactions in the bed and the thermal properties of the material.

There are several ways of modelling the characteristics of the granular bed. The simplest way is to assume that the material bed is perfectly mixed and use the temperature profile of the freeboard model in order to use it as input for a one dimensional model of chemical reactions of the following or similar form.

$$\frac{dC_i}{dz} = f(T, C_j), \tag{1-1}$$

where z is the axial direction of the kiln, T the temperature, and C_i is the concentration of the i^{th} species. For more information on reaction kinetics, refer to [28, 13]. This approach is used by Mastorakos, Li, Mujumdar [32, 29, 35] and similarly by Kääntee [22]. This is equivalent to have a 1-D model of a Plug Flow Reactor (PFR) in the solids phase.

The main advantage for this approach is that one only needs to solve a system of ordinary differential equations with data from a freeboard model. It treats the granular bed as if it was a packed bed reactor. This type of reactor is extensively studied in the field of chemical engineering [13, 28, 26] and by using this approach and reaction kinetics from experimental data one can get good qualitative results [22]. If an energy balance is included, one can couple the energy exchange between the particle bed and the freeboard due to chemical reactions [32].

The main disadvantage of this approach is that the particle bed is usually not very well mixed, thus results could differ greatly from reality. This is normally the case, as this approach is

used primarily for the finding of qualitative trends on changes of parameters or feed of a rotary kiln such as Kääntee does in her paper [22]. It is interesting to note, that Kääntee uses Aspen Plus [2] to simulate the chemical reactions involved in the freeboard and particle bed, contrary to Mastorakos [32] who couples a CFD solution for the combusting gases in the freeboard with a bed model based in the solution of mass and energy conservation equations. By using Aspen-plus Kääntee also assumes a PFR behaviour on the freeboard.

There is not much information on coupled simulations for the granular bed of a rotary kiln. However, there are various publications that describe models for hydrodynamics and heat transfer in the transversal plane for the kiln. Heydenrich proposes in his PhD thesis [19] some interesting models in the transversal plane for heat and mass transfer in rotary kilns with a rolling mode, however, there is no indication that it could be useful in a practical sense. Boateng [6] presents a model for the transversal plane hydrodynamics based on kinetic theory of gases applied for dense granular flow in a two fluid approach. He makes the distinction between the plug flow layer and the active layer and defines a transfer coefficient between the layers. The main downside is that his model does not work well with kilns with low loading, which leads to the assumption that such model is only qualitatively good.

In the present work, due to the low loading of the studied rotary kiln, a one-dimensional PFR approach will be followed for heat transfer and chemical reactions. Furthermore, a two-dimensional continuum transversal heat transfer model will be attempted using granular bed velocity fields calculated from a granular motion model.

1-4 Transverse and Axial Granular Bed Motion

There are two mixing mechanisms in a rotary kiln, an axial and a transversal component [6]. The axial mixing component is attributed to overall convection; one can assume that there is an average velocity equal to the plug flow velocity. However for the transversal or radial mixing, one has mechanisms that result in velocity components in both axial and transversal directions.

Both are dependent on the rotation, inclination, filling percentage of the kiln and rheological properties of the material to be processed. Both mixing mechanisms increase with kiln rotational speed [6].

As it can be inferred from the previous statements, movement of the particle bed inside the rotary kiln has two components: the axial component that determines the residence time and the transverse plane component that determines most of the transport processes such as, mixing, heat transfer and reaction rate.

1-4-1 Transversal Bed Motion

There are various studies that describe the motion of particles in a rotating cylinder. They show that the motion depends on the dimensionless Froude number [17, 18].

$$Fr = \frac{\omega^2 R}{g}, \tag{1-2}$$

where ω is angular velocity in $[s^{-1}]$, R is the radius of the kiln in $[m]$ and g is the gravity in $[m/s^2]$.

Henein and Boateng noted six different transversal motion modes for rotary drums as shown in Figure 1-3 [6, 17]:

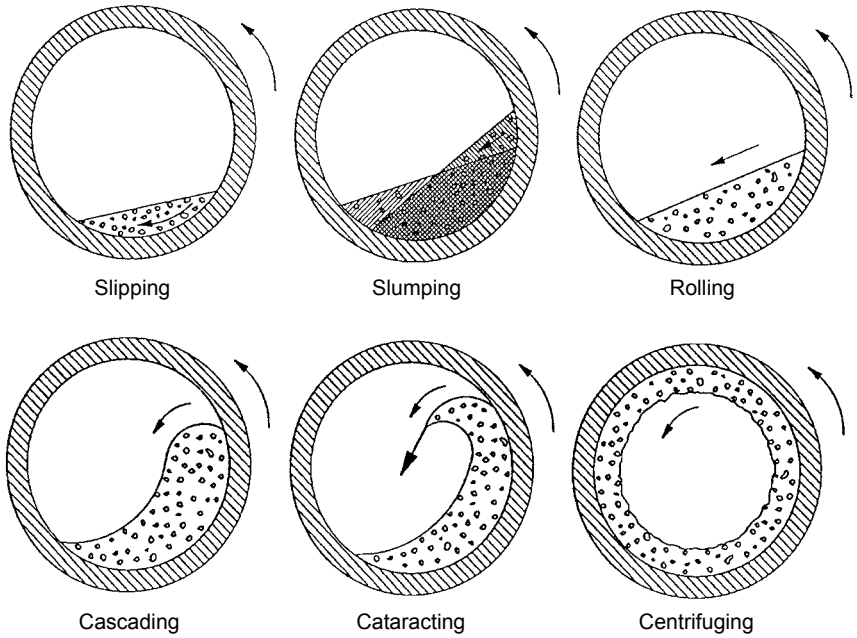

Figure 1-3: Different modes of operation in the transversal mixing plane of a rotary drum [6]

The description of the transversal modes from low to high Froude number is as follows:

- Slipping: occurs when the bulk material, as a whole, slips against the wall;
- Slumping: occurs when a segment of bulk material at the shear wedge becomes unstable, yields and empties down the incline;
- Rolling: occurs when there is a steady discharge onto the bed surface causing its renewal;
- Cascading: occurs at high rates of rotation, where the particles cascade or shower down the free surface;
- Cataracting: occurs in between cascading and centrifuging mode;
- Centrifuging: occurs at critical and high speeds, all the material rotates with the drum wall.

Henein in his research developed graphs with experimental data in order to characterise the mode of operation depending on operating parameters and geometry aspects of rotary drums [18].

For the studied kiln the Froude number is of the order of $Fr = 10^{-4}$. Then by comparing the operating conditions and Froude number with the figures presented by Henein in his paper

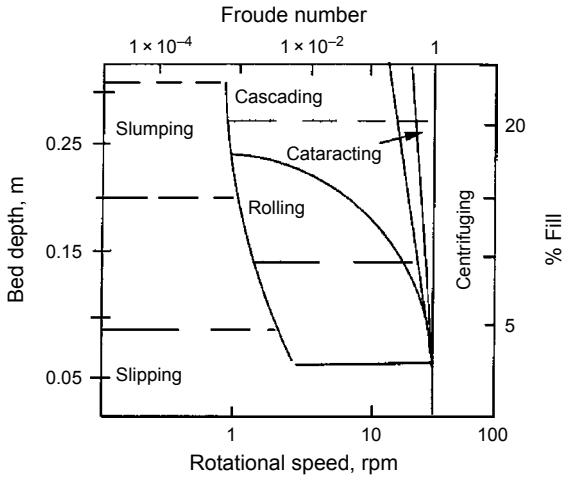

Figure 1-4: Characteristic curve for a 0.40 diameter rotary drum [6, 18]

from 1983 [17] similar to Figure 1-4, it can be inferred that the operation of the kiln lies in a region between slumping and rolling mode. However, one must make the distinction that the particle sizes and properties from the study are not the same as in the case of the particular rotary kiln to be analysed. Thus, as it is shown in later chapters, it is imperative to conduct further research in order to characterise the transversal flow of the kiln.

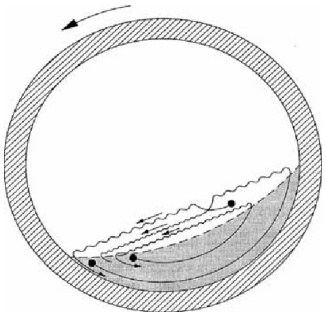

Figure 1-5: Rolling mode with an active top part and a passive lower part [6]

Rotary kilns usually operate with a rolling mode, as it is the mode where the mixing is maximised [6]. A maximal mixing is when a mixture of material is homogeneous, which in turn means that the material has a uniform composition and temperature. Thus, the previously mentioned flow mode will be described as its description is useful when analysing results in coming chapters.

When a kiln is operating in rolling mode there are two areas that can be described: an active layer near the top where a surface renewal occurs from the rolling motion of the particles falling down, and a passive layer, which is beneath the active layer and assumed to have a plug flow behaviour.

Most of the mixing in the kiln cross section occurs in the active region. Taking into account the surface renewal in the active layer, one can infer that by increasing the rotational speed of the kiln one can get better mixing. However, this will decrease residence time as axial

speed increases with increasing rotational speed. Thus, it is important to know the critical residence time to achieve the sufficient product quality in order to have a balance between mixing and residence time [6]. The developed one-dimensional kiln model can be used as an aid to define the critical residence time needed to achieve full conversion of its reactants.

1-4-2 Axial Bed Motion

Boateng [6] mentions that the best way to define axial bed motion is by using empirical relationships based on geometric considerations. He concludes that a reasonable assumption is to take into account an average axial flow based on the average residence time.

1-5 Heat Transfer Phenomena

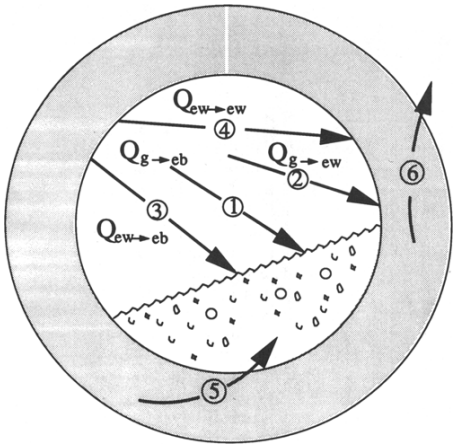

Figure 1-6: Kiln basic heat transfer paths: 1) Freeboard gas to exposed bed, 2) Freeboard gas to exposed wall, 3) Exposed wall to exposed bed, 4) Exposed wall to exposed wall, 5) Covered wall to covered bed, 6) Loss to surroundings [9].

Brimacombe [8, 9] explains that there are three basic paths of heat transfer into the particle bed:

- Freeboard gas to exposed bed;
- Exposed wall to exposed bed;
- Covered wall to covered bed;

where for the first point there are two mechanisms, the radiative heat transfer and the convective heat transfer from the gases to the bed. For the second point there is only one mechanism, the radiative heat reflected from the wall to the bed. And lastly, the mechanism is given by conductive heat transfer from the wall to the particle bed.

From all the mechanisms, Boateng [6] mentions that the main heat transfer path is the radiative heat transfer from freeboard to the bed. In Figure 1-6 the basic paths for the heat transfer of a kiln cross section are presented.

As mentioned in previous sections heat transfer mechanisms within the bed are the same as in packed beds. This means that it is mainly given by particle to particle conduction [6]. This makes the heat transfer modelling within the particle bed relatively simple in discrete or continuum models.

1-6 Chemical Reactions

As mentioned in previous sections, the chemical reactions occurring in the studied kiln are sintering reactions. In a sintering process, particles grow and adhere to each other forming different phases [23]. In the present work, the Calcium Aluminates phase diagram will be considered as shown in Figure 1-7.

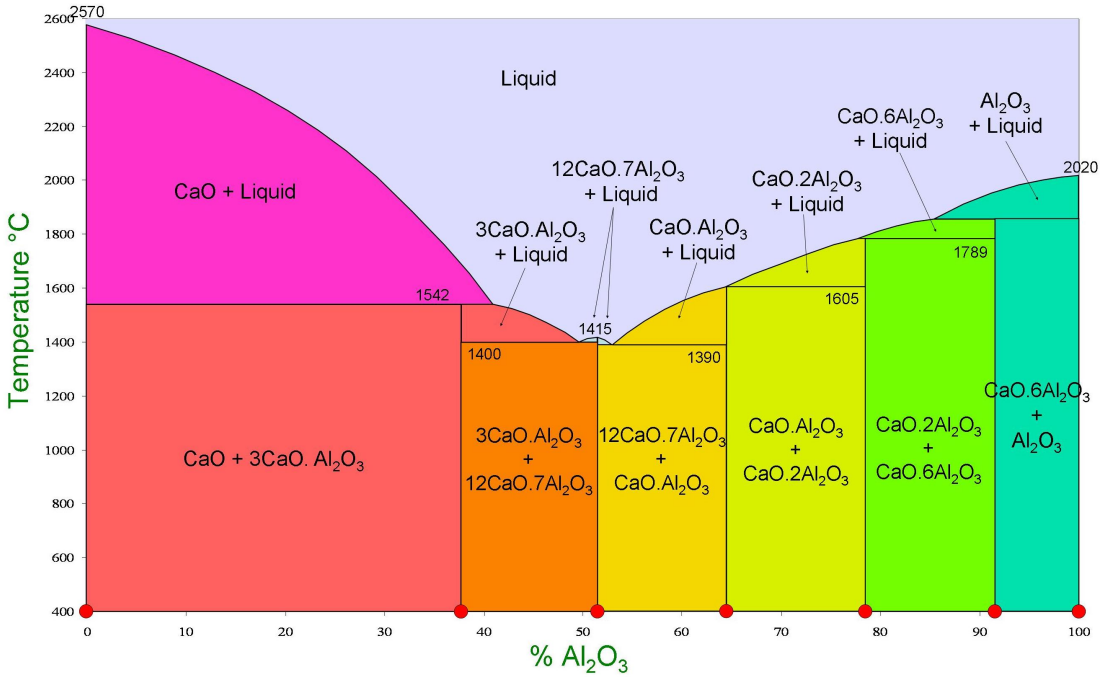

Figure 1-7: Phase Diagram for Calcium Aluminates

It can be observed on the phase diagram the dependence of the phase compositions to the temperature. By observing Figure 1-7 one can also remark the importance the temperature has on the final product at the end of the kiln.

One then can note that the chemical reactions occurring in the kiln can be described as follows:

$$\gamma CaO(s) + \alpha Al_2O_3(s) \rightarrow \gamma CaO \cdot \alpha Al_2O_3(s). \tag{1-3}$$

Further details will be given with the development of the chemical reaction model for Calcium Aluminate Cement in Chapter 3.

1-7 Scope of the Project

One can divide the current project into three distinct parts:

- The first being the granular flow modelling which is attempted as described by the literature with an Euler-Euler [45, 14, 36] and an Euler-Lagrange DEM approach [43, 42, 25].
- Secondly, the development of a one-dimensional axial kiln model including chemical reactions following similar approaches found in the literature [6, 35, 29, 32], proposing chemical reaction kinetics from experimental XRD data [20, 34, 24] and solving the resulting DAE system [33].
- Finally, the development of a transversal granular bed heat transfer model based on a volumetric heat balance on the bulk solids [6] taking into account the results from the first and the second point, and by consequence solving a PDE [33].

All three points have particular conclusions with regard to the modelling of a rotary kiln and to practical considerations related to the studied industrial kiln.

It is to be mentioned that there is a collaboration with Dr. D. Van Puyvelde [41, 47] in writing a journal article concerning the work done in the present document.

Chapter 2

Transversal Granular Flow Model

Rotary kilns are used to process granular material. Granular material is a collection of solid particles, in which every particle is in contact with at least some of the neighbouring particles. This granular material has transport properties similar to both liquids and solids [43]. One calls granular flow the movement of such material.

Two typical ways of modelling granular flow are presented [43, 40]:

- Discrete Method: Euler-Lagrange approach (Coupled DEM)
  - Treat the material as a collection of particles. Newton′s laws of motion are applied to each particle.
- Continuum Models: Euler-Euler approach (Two fluid modelling)
  - Particles are modelled as a continuous medium where all the quantities are assumed to be smooth functions of position and time.

Both of them are valid and have advantages and disadvantages. In the following sections both approaches will be explained and referrals to its validity for rotary drums will be given.

2-1 Euler-Lagrange Approach: Discrete Element Modelling

With this approach each particle is simulated by applying Newton′s laws of motion and are followed in time [43, 42]. For particle tracking one then has the following governing equations,

$$\frac{dx_{p,i}}{dt} = u_{p,i} \tag{2-1}$$

$$\frac{du_{p,i}}{dt} = \frac{1}{m_p}\sum F \tag{2-2}$$

where $x_{p,i}$ is the position of the particle, $u_{p,i}$ the velocity of the particle, m_p the mass of the particle and $\sum F$ the sum of forces exerted on the particle, respectively.

This set of equations is also known in the literature as the Basset-Bousinesq-Oseen equations [11, 40] when fluid-particle interactions are taken into consideration.

The sum of forces depend on various factors such as drag, lift, gravity, buoyancy, contact, friction and so on. Usually one can make assumptions in order to include or not certain forces depending on the type system to be modelled.

The method consists of calculating the F forces and then solving the set of ordinary differential equations described above. By adding other equations per particle, such as an energy and material balance, one can have particle properties included in the ODE set and calculate for a certain time the position, velocity, temperature and mass, concentration or diameter of the particle [42, 40].

One of the main points to be considered is the computation of the contact forces. For granular flows a soft sphere approach is used. This consists in letting the simulated particles overlap. This overlap can be seen as the displacement of a spring. Then one can use a relation similar to Hooke′s law in conjunction with a dampener model, used to model energy dissipation due to contact, to compute the contact forces.

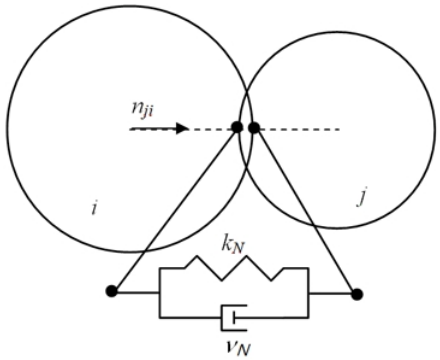

Figure 2-1: Spring and damper contact force model

The soft sphere approach is also known as the spring and damper model which can be observe in Figure 2-1. Usually one uses a non-linear spring model. This means solving an additional set ODE per particle as one has to have into account contact on all neighbouring particles. For these models, one needs certain physical properties of the particles such as the restitution coefficient. Refer to Radjai′s book [42] for more information on the modelling of contact forces.

2-1-1 Applicability to Current Problem

There are various papers that deal with discrete element simulations for rotating cylinders [27, 47, 12, 41, 44, 49]. However there is no paper which describes a complete model for a rotary kiln. All of them agree within a certain degree that a DEM (discrete element method) approach is valid for the type of granular flow exhibited in a rotary kiln. Kwapinska [27] for instance, validates the transversal mixing of a DEM approach with data from Van Puyvelde

[47], whose experimental results are cited for its value within the characterisation of mixing of rotating drums. Kwapinska then concludes that the DEM approach, with certain tweaks, can be much better than the existing continuum models for rotary drums with respect to mixing and hydrodynamics in the transversal plane [27].

In a more recent paper by Van Puyvelde [41], the author remarks using data existing in literature [47, 17, 18] for the calibration of the DEM method with respect to this specific problem. Refer to Radjai [42] for information on the parameters for the calibration of the DEM for dense granular flow.

These publications indicate that a discrete approach is valid for a rotary kiln. This then bring us to consider the size of the problem. It is well known from the cited literature that this kind of model is computationally expensive for a high number of particles.

2-1-2 Discussion: Advantages and Disadvantages

As described in the previous section, DEM simulations can turn out to be computationally expensive. They do, however, have the following advantages:

- Simple to model and easy to understand physics
- Relatively easy to implement and there are already a number of commercial and open source implementations: Star CCM+, OpenFOAM, LIGGGHTS/LAMMPS, MFIX [10, 36, 25, 45]
- All of the implementations presented above can run in parallel

The first point is proved in the previous sections. On the second point a short research on software capabilities was done. From the options presented, all have DEM, coupled CFD-DEM capabilities and can run in parallel. This is desirable because one then has to care about tweaking and not so much about coding.

For the disadvantages a list is also presented:

- Computationally expensive
- Still needs empirical adjustments

As described in the literature, the method is valid for kiln slices. Thus the method is to be used in later sections of the current chapter.

2-2 Euler-Euler Approach: Two-Fluid Model

Two-phase hydrodynamic models treat the fluid and the solids phase as two interpenetrating continua. It is an averaging approach where equations are derived by space, time or ensemble averaging of the local instantaneous balances of each of the phases. In other words, it is a Reynolds-Averaging Navier-Stokes approach [45].

These models occur due to the increase of interest for the scale up for operations involving fluidized beds, packed beds, and so on [45, 14]. They use analogies from kinetic theory of gases in order to model the solids phase. One of the classical text books with applications for fluidisation is written by Gidaspow [14]. The same approach could be used in order to model the rotary kiln, thus a description of the governing equations will be presented.

The following description will be based on the MFIX Theory Guide written by Syamlal which is basically a review and a general overview of the Euler-Euler Approach [45]. The document is usually referred to in online tutorials for the understanding of the theory behind the Euler-Euler Approach. The equations presented next are the most important from the described document.

First of all, due to the averaging of variables one must assume that the point variables are averaged over a region that is large compared with the particle spacing, but smaller than the flow domain. One then introduces new variables, the volume fractions of the phases which are assumed to be continuous functions of space and time:

$$\sum_{\alpha \in P} \varepsilon_\alpha = 1, \tag{2-3}$$

where P is the set of phase indices. For simplicity only two phases will be considered, a solids phase s and a gas phase g. One then has:

$$\varepsilon_g + \varepsilon_s = 1. \tag{2-4}$$

Then by considering the conservation of mass in the gas and solids phase:

$$\frac{\partial}{\partial t}\left(\varepsilon_g \rho_g\right) + \nabla \cdot \left(\varepsilon_g \rho_g \overrightarrow{v_g}\right) = R_g, \tag{2-5}$$

$$\frac{\partial}{\partial t}\left(\varepsilon_s \rho_s\right) + \nabla \cdot \left(\varepsilon_s \rho_s \overrightarrow{v_s}\right) = R_s, \tag{2-6}$$

where the ρ denotes the bulk density of the phases, $\overrightarrow{v}$ the phase velocity vector, and R the rate of production of the phase (or mass transfer between the phases). These are the continuity equations for the gas and the solids. One needs an additional equation of state for the gas. This could be the ideal gas law or any other equation of state for real gases.

For the conservation of momentum one gets the following:

$$\frac{\partial}{\partial t}\left(\varepsilon_g \rho_g \overrightarrow{v_g}\right) + \nabla \cdot \left(\varepsilon_g \rho_g \overrightarrow{v_g}\overrightarrow{v_g}\right) = \nabla \cdot \bar{\bar{S}}_g + \varepsilon_g \rho_g \overrightarrow{g} - \overrightarrow{I}_g, \tag{2-7}$$

$$\frac{\partial}{\partial t}\left(\varepsilon_s \rho_s \overrightarrow{v_s}\right) + \nabla \cdot \left(\varepsilon_s \rho_s \overrightarrow{v_s}\overrightarrow{v_s}\right) = \nabla \cdot \bar{\bar{S}}_s + \varepsilon_s \rho_s \overrightarrow{g} + \overrightarrow{I}_g. \tag{2-8}$$

It can be observed that the balance of momentum presented above is exactly the same as the one presented in literature for basic fluid dynamics [4]. The first term in the left hand side is the rate of increase of momentum per unit volume, the second is the rate of momentum

addition by convection per unit volume where $\overrightarrow{v_s}\overrightarrow{v_s}$ denotes the dyadic product of two vectors. On the right hand side the first term is the rate of momentum by molecular transport per unit volume given by the stress tensor $\bar{\bar{S}}$. The second and third term are the external forces on fluid, where the gravity vector can be observed given by $\overrightarrow{g}$ and the by the interaction forces (momentum exchange) between phases given by $\overrightarrow{I}$.

The interaction forces between phases can be modelled in the same way as in the Euler-Lagrange approach using drag, buoyancy and mass transfer:

$$\overrightarrow{I}_g = -\varepsilon_s \nabla P_g - F_g \left(\vec{v}_s - \vec{v}_g\right) + R_0 \vec{v}, \tag{2-9}$$

where $R_0\vec{v}$ is the momentum transfer due to mass transfer, ∇P_g is the pressure gradient of the gases and F_g describes the drag forces caused by the gas. Numerous expressions exist for these interaction terms, these can be seen in the document by Syamlal and the book from Gidespow [45, 14].

It can be noted that the stress tensors for the momentum equations are missing for both phases. For the gas phase the stress tensor takes the form of a Newtonian Fluid, which one can find in any fluid mechanics and transport phenomena book [4]. However for the solids stress one needs an analogy to adopt theories for the description of granular flows. Granular flows can show characteristics from both solids and liquids, thus it has been proposed that most of its dynamic behaviour has analogs in other systems [21, 43].

Granular flows can be classified in two regimes, a plastic flow which is slowly shearing and a viscous flow which is rapidly shearing. This brings two different approaches to describe the solid stresses. For the plastic flow, an empirical power law from soil mechanics is usually in place. For the viscous flow, an analogy with the kinetic theory of gases is used, where there is momentum transfer due to the kinetic energy in that comes from particle collisions. In this case the stress tensor would be dependent on a granular temperature, which comes from an additional PDE, and a bulk viscosity term which in the present case would be based on the one presented by Lun et al. for dense granular flow. For the details on the solids phase stress tensor we refer to the publications from Gidaspow, Syamlal and Lun [45, 14, 30]. For an introduction to the concept of granular temperature we refer to the paper from Goldhirsch [15].

2-2-1 Applicability to Current Problem

For the applicability of a two fluid approach on rotary kilns, one can consult the publications from Boateng [6, 5]. He develops a model for the transversal plane of a kiln taking as a base the same governing equations as above. The model only solves for the active layer as the passive layer is assumed to be non-shearing. He achieves success using his model for kiln loads higher than 10%. For kilns that are not as loaded, there is some discrepancy from experimental data.

From recent advancements in code and correlations for Euler-Euler multiphase modelling of granular flow one can assume that they could be valid for the transversal plane of a rotary kiln. This can be done by adopting models which are valid for slowly and rapidly shearing granular flow or by switching to stress tensor correlations depending on the packing of the

solids phase [6, 45]. This makes a rotary kiln model possible as the plug flow layer is slowly shearing and the active layer is rapidly shearing. However, as Lun [30] notes for Euler-Euler modelling of granular flow, one usually needs empirical adjustments depending on the case to be modelled.

2-2-2 Discussion: Advantages and Disadvantages

As with the DEM approach, a Two-Fluid model pose a number of advantages. The following summary can be done:

- Less computational cost than the DEM approach [40]
- Chemical reactions easy to include
- There are existing commercial and open source eulerian solvers such as: Star CCM+, OpenFOAM, Fluent, MFIX [1, 10, 36, 45]

For the first point one must note that solving a problem using a RANS code is equivalent to solving a system of coupled PDEs with the finite volume method. The speed depends on the spatial discretisation, more specifically the number of cells. It must be noted that the number of cells will be far less than the number of particles. As for the chemical reactions, because of the nature of the finite volume approach, this is equivalent to a number of CSTRs (Continuos Stirred-Tank Reactors) in series and parallel, which in turn is equivalent to a PFR/PBR (Plug Flow Reactor/Packed Bed Reactor) [13, 28]. This makes the inclusion of chemical reactions easy if experimental data is in hand.

As for the disadvantages:

- Much more complicated to understand and to set up
- Only reported to be valid for rotary drums in rolling mode [7]

The first point can be made obvious by the length to the introduction of the theory of an Euler-Euler approach. As for the tweaking, this is usually discussed while presenting or explaining the approach [40, 45, 17, 30]. Authors agree that the described approach requires tweaking based on experience and experimental observations.

2-3 Summary: Euler-Lagrange and Euler-Euler

In the previous sections two approaches for the modelling of granular flow were presented. Both have some similarities and differences, as well as advantages and disadvantages.

Concerning similarities, the easiest to appreciate is given by the phase interactions. In the Euler-Lagrange approach one can observe in Equation 2-2 that the sum of forces exerted on the particle are given by drag, lift, gravity and buoyancy correlations. On the other hand, by carefully examining Equations 2-7 and 2-8 one can see that there is also an interaction term

given by the momentum transfer between phases. The interesting observation is that this interaction term is given by the same correlations for drag, lift, gravity and buoyancy forces that are used in the Euler-Lagrange approach [40, 11].

Other similarities reside in the fact that both approaches can be used either for dispersed multiphase flow and dense granular flow [40, 11, 43].

For the differences, the most obvious is the fact that the Euler-Lagrange approach involves the modelling of every particle and the Euler-Euler approach involves the modelling of volumes of a number of particles. These differences can be broken down into advantages and disadvantages. In Table 2-1 a summary of both approaches is presented.

	Advantages	**Disadvantages**
Euler - Lagrange	Relatively easy to set up, it is proven to work for rotating cylinders	Can turn out computationally expensive
Euler - Euler	As it is a RANS code, it can run as fast as any multiphase CFD code, chemical reactions are easily incorporated	Complicated to set up and tweak

Table 2-1: Summary of advantages and disadvantages for the discussed modelling approaches to granular flows

In order to characterise the transversal flow of the rotary kiln in question, two models were set up in order to explore which approach would be feasible for a rotary kiln model. In the coming section, results will be presented and discussed concerning both, a Continuum approach and a DEM approach.

2-4 2-D Granular Flow Model

2-4-1 Euler-Euler Two-Fluid Model: Experimental Setup and Results

A short experiment was done in order to try to build a rotating drum Euler-Euler model in OpenFOAM [36] to check feasibility. Tutorials on two phase Euler simulations for fluidized beds were followed with changes being done to adapt it to a rotary drum simulation. A summary of the parameters of the simulation is done next:

- A kinetic theory description with correlations from Lun [36, 30] for dense granular materials was used
- Material properties from CaO were used
- A normal velocity with respect to the cylinder wall was defined as a boundary condition for the granular phase
- A non-uniform grid was used using BlockMesh from OpenFOAM

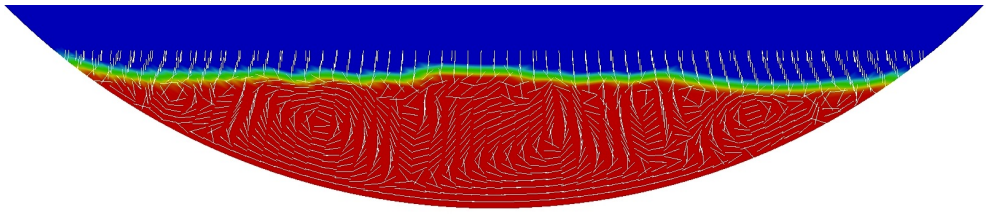

Figure 2-2: OpenFOAM Euler-Euler Model Results

As it can be observed from Figure 2-2, the flow field calculated by the model does not describe correctly the granular flow modes described by Boateng [6]. There is a hint that the inconsistencies are due to inherent problems in two phase Euler modelling in OpenFOAM which are being addressed by Passalacqua in his paper from 2010 [37]. He states that there is a stability problem with simulations with packings near the limit (as it is the case in the passive layer of a rotary kiln). This was confirmed by the experiments which were done above and by a user forum discussion in CFD Online about OpenFOAM and high packing two phase Euler modelling.

By recalling the behaviour diagrams from Henein [18] presented in Chapter 1, there is an indication that when having a kiln with low loading, as it is with the case with the kiln in question, the transversal flow mode is unclear. The diagrams lead to the conclusion that the assertion that the bed is in rolling mode is questionable. Due to this remark, the inability to run a Two-Fluid approach with OpenFOAM may not be only due to numerical limitations.

As it will be shown on the next section, it may be the case that the transversal flow mode of the analysed kiln is not in rolling mode but in a slumping mode. The mentioned mode which exhibit transient characteristics which were not found to be typically modelled with an Euler-Euler approach.

2-4-2 DEM Model: Experimental Setup and Results

As mentioned in the previous section, the behaviour diagrams from Henein [18] hint that the studied kiln is not in rolling mode. Thus, numerical experiments using a DEM model to analyse the transient characteristics of the granular flow is used.

The geometry for the experiment was set up as follows, 2-2.5 m diameter cylinder with 3 particle diameters length in the axial direction, a rotation of 1.5-2 rpm and a periodic boundary condition in the axial direction. The diameter and rotational speed correspond to the studied rotary kiln. The particle size was varied from 1 mm to 5 mm. The smaller particle sizes were discarded to ease computational cost as the aim is to gain qualitative understanding. The friction factors of both granular walls and granular material were varied from 0.5 to 0.95. Other parameters such as the Young Modulus were selected from physical properties of Calcium Aluminates found in the literature.

The results from the experimental run with friction factors of 0.8 and particle sizes of 4 mm will be presented due to the fact that the characteristics of the granular motion are easily observed on this experimental run. It is important to note that the same qualitative

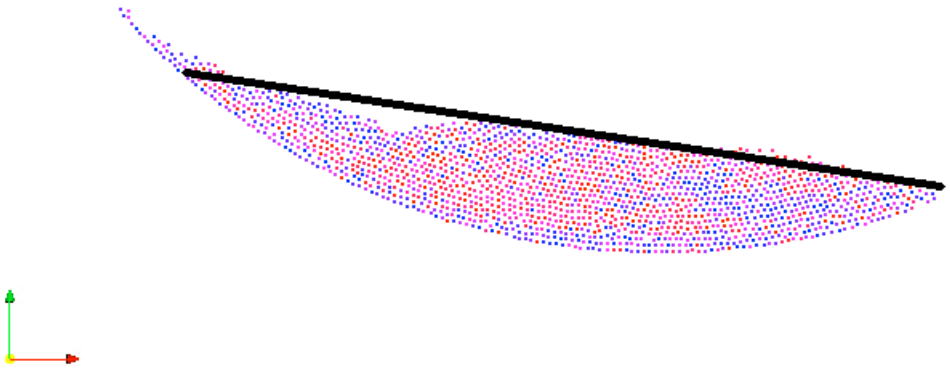

(a) Time-step 730

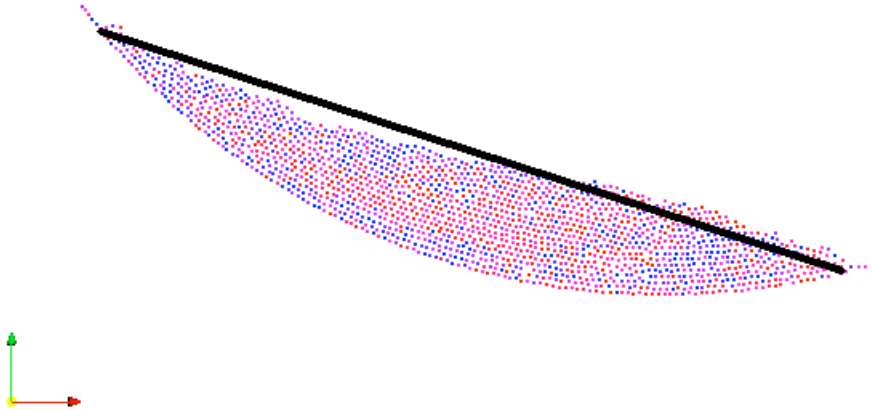

(b) Time-step 835

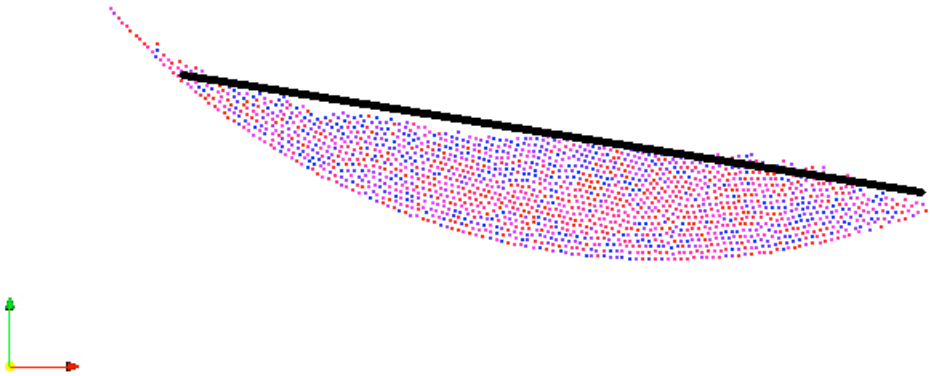

(c) Time-step 950

Figure 2-3: DEM Run: 4mm, 0.8 friction. Slumping Mode, a) Time-step 730, b)Time-step 835, c) Time-step 950

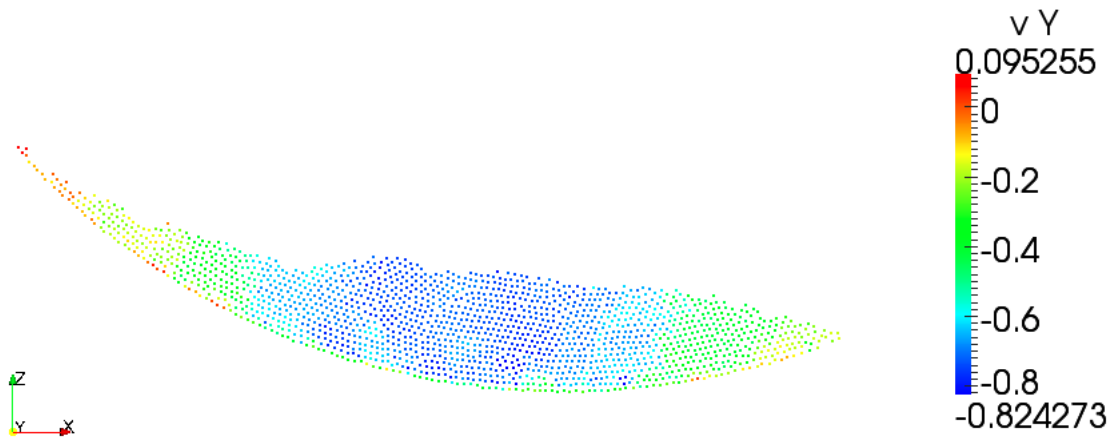

(a) Time-step 730

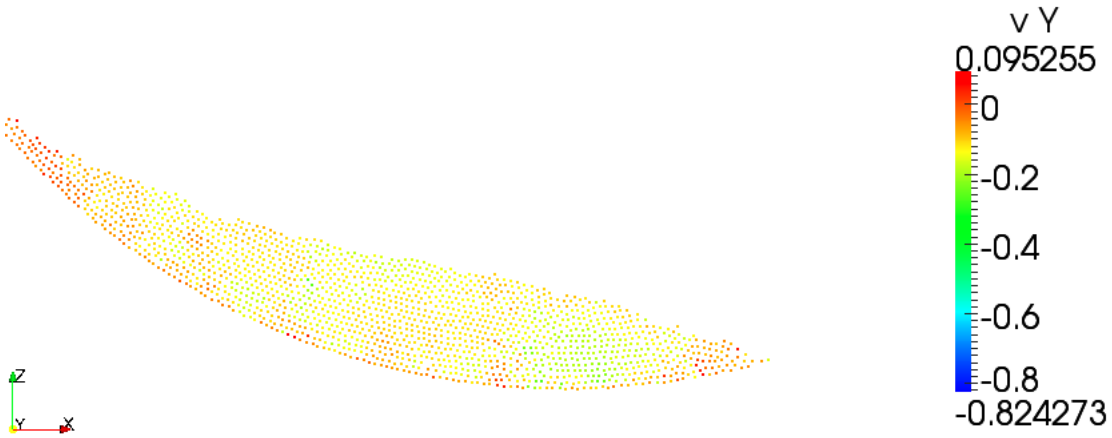

(b) Time-step 835

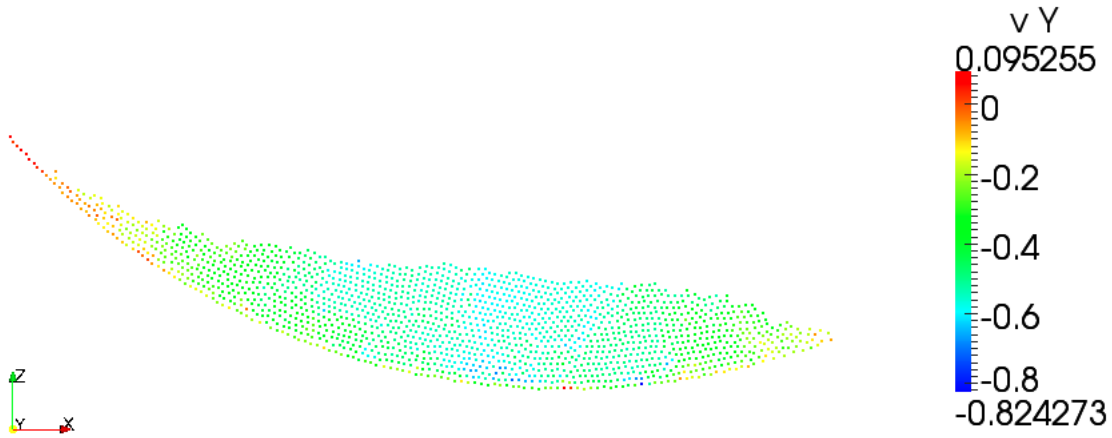

(c) Time-step 950

Figure 2-4: DEM Run: 4mm, 0.8 friction. Axial Velocity Magnitude, a) Time-step 730, b)Time-step 835, c) Time-step 950

characteristics were observed in all experimental runs, independent of the friction factors and particle size.

Recalling the definition of the slumping regime presented in Chapter 1: slumping occurs when a segment of bulk material at the shear wedge becomes unstable, yields and empties down the incline. As one can observe from Figure 2-3, there seems to be a slumping regime on the granular motion in the cylinder. The black lines were superimposed to aid the observation of the slumping motion. In addition to the increasing angle observed with the black line in Figure 2-3, when the material rolls down there is a velocity increase in the axial direction. The previously described phenomena can be observed in Figure 2-4 with the axial velocity magnitude colouring.

The described characteristics were observed in every experimental run using the model. This fact brings a number of implications to the present work. At a first glance, further work must be done in order to gain more understanding about the slumping regime, as there is practically no information on the literature with a detailed description. Secondly, it is imperative to prove whether the bed can be modelled as a perfectly mixed continuum, even knowing that it is probably in the slumping regime. Lastly, having a slumping regime means that due to the periodicity of the slumping movement there cannot be a steady state solution for the velocity fields.

2-5 Conclusions

As observed in the previous section, an Euler-Euler model is not possible to set up with OpenFOAM using the operating parameters of the studied rotary kiln. This could be due to inherent numerical problems due to high packing or due to the transient behaviour of granular flow modes which has not been found reported to be valid for rotating drums.

However, a DEM model seems to be appropriate for transient behaviour as there are hints in the literature that the approach is able to model different transverse granular flow modes in rotating cylinders [12]. It is to be noted that due to the non-sphericity and lack of experimental data, the results from the DEM are to be taken qualitatively.

From the results from the DEM model on the previous section, one can infer that the studied kiln is probable not in rolling mode but in a slumping mode. From a practical perspective, this means that product uniformity in the kiln is not optimised. This should be taken into account when designing further kilns, as better transversal mixing correlates to product uniformity. This is much better described in Chapter 4 with the transversal heat transfer model for the granular bed.

Chapter 3

One-dimensional Kiln Model: Heat Transfer and Chemical Reactions

In the present chapter a rotary kiln one-dimensional model is to be developed for the Calcium Aluminate Cement Rotary Kiln from the Industrial Partner for which there is an existing CFD Freeboard model. Data provided from the mentioned model will be used as initial conditions. Calibration was done by taking temperature measurements at the Industrial CAC plant.

The one-dimensional kiln model encompasses two phenomena in the kiln. The axial heat transfer and the sintering reactions occurring in the bed. In the present chapter, a one-dimensional axial heat transfer model is developed and validated with data from the literature [3] and a sintering reaction kinetics model is developed taking as a basis information found in literature and experimental XRD (X-Ray Diffraction) data handed by the industrial partner [24].

Furthermore, the developed one-dimensional kiln model is used to analyse two different air to gas fuel ratios and its consequences with respect to the production of CAC. It was found that the developed model was in accordance to the observations made by the industrial partner with respect to the quality of the product from the kiln. It was observed that for the case of Air to Gas ratio of 12 the production was better than the case of Air to Gas ratio of 9. By using the developed model one can conclude that the discrepancies in product quality between the mentioned cases is probably due to side reactions occurring in the case of Air to Gas ratio of 9 because of a fast conversion of Alumina.

3-1 Model Assumptions

One starts by considering the following assumptions:

- the freeboard gases are perfectly mixed in the transversal plane,
- the granular material temperature is uniform in the transversal plane,

- the granular material flows as a PFR with a mean residence time in the Kiln,
- the granular material is in thermal equilibrium with the freeboard gases.

For the freeboard gases, homogeneity is questionable due to the fact that the CFD freeboard model does not show perfect temperature uniformity. However, one uses an axial average of the freeboard temperature achieving good qualitative results.

Due to the low loading of the kiln and the high temperatures, the assumption of granular bed transversal temperature uniformity seems correct if there is a sufficient mixing in granular material in the transversal plane.

The granular flow taken as a PFR (Plug Flow Reactor) is an assumption commonly associated with one-dimensional kiln models [6, 35, 29, 32]. It is a direct consequence from the axial flow determined by an average residence time.

Lastly, the thermal effect that the bed has on the freeboard can be neglected due to the low loading of the kiln, thus it seems reasonable to assume that the bed is in thermal equilibrium with the freeboard. This assumption is also stated in the approach by Li for Portland Cement Kilns [29] with validated results for industrial size kilns and pilot-scale kilns.

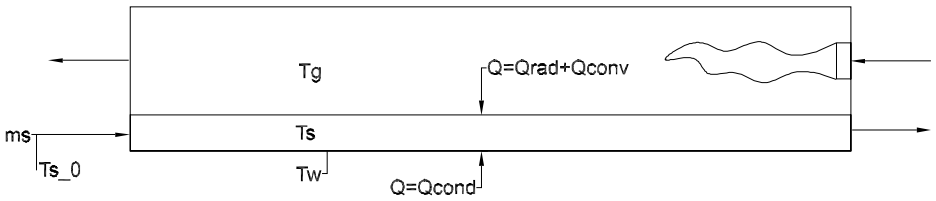

(a) 2-D Kiln Sketch

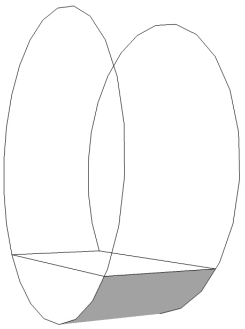

(b) Differential Volume of the Granular Bed

Figure 3-1: 2-D Scheme of the kiln and Differential Volume of the Granular Bed. Tg denotes gas temperature, Ts bulk solids temperature, Tw wall temperature, ms bulk solids mass flow, Ts_0 bulk solids temperature at feed, Q heat transfer into bulk solids, $Qrad$ heat transfer due to radiation, $Qconv$ heat transfer due to convection and $Qcond$ heat transfer due to conduction.

One then considers a differential volume in the bulk solids and performs an energy balance:

$$\dot{m}_s c_{p,s} dT_s = q dA \quad [W], \tag{3-1}$$

where the left hand side denotes the heating of the bulk material and the right hand side the heat transferred to the material at position z. It is to be noted that the heat transfer paths are the same as described in Chapter 1.

By rearranging the terms one gets the following:

$$\dot{m}_s c_{p,s} \frac{dT_s}{dz} = q L_{crd} = \frac{Q L_{crd}}{A} = \frac{Q}{L_K} \quad [Js^{-1}m^{-1}], \tag{3-2}$$

where $\dot{m}_s$ is the mass flow rate, $c_{p,s}$ the heat capacity of the solids, T_s the temperature of the bulk solids, q the heat flux into the bulk solids, Q the heat transfer rate, L_{crd} the chord length for calculating the area of heat exchange, A the heat exchange area between freeboard and granular bed, and L_K the total kiln length.

It is to be noted that implicit in the heat transfer rate Q shown above are the heat transfer paths described in Chapter 1. By noting this, one can observe that Equation 3-2 can also be seen as the governing equation of the axial heat transfer model.

In the following sections expressions for the heat transfer paths described in Chapter 1 will be shown. It is to be noted the following adjustments in nomenclature with respect to Figure 1-6 and the present chapter:

$$\begin{aligned} Q_{g\to eb} &= Q_{radiation,g\to s} + Q_{convection,g\to s}, \\ Q_{g\to ew} &= Q_{convection,g\to w}, \\ Q_{ew\to eb} &= Q_{radiation,w\to s}. \end{aligned}$$

On the left hand side one can observe the nomenclature given in Figure 1-6 and on the right hand side one can observe the nomenclature used in the present chapter.

One should note as well that the nomenclature used in the present chapter will be in accordance to mechanical and chemical engineering texts where a heat transfer coefficient is used. We note that the heat transfer rate can be written as [4]:

$$Q = hA\Delta T,$$

where Q is the heat flow [W], h the heat transfer coefficient [W/m^{2}K], A the heat transfer surface area [m^2] and ΔT the temperature difference between two materials [K].

3-2 Radiative Heat Transfer

In the present section models considering radiative heat transfer within the kiln will be presented.

A simplified radiation model considering the radiation from the freeboard presented by Mujumdar in his 2006 paper [35] is shown next. The following equation is valid for emissivities fulfilling $\varepsilon > 0.8$:

$$Q_{radiation,g\to k} = \sigma A_{g\to k}(\varepsilon_k + 1)\left(\frac{\varepsilon_g T_g^4 - \alpha_g T_k^4}{2}\right) \quad [W], \tag{3-3}$$

where the subscript $k = w, s$ represents the gas or the solids phase respectively, σ is the Stefan-Boltzmann constant, A is the area of heat transfer, ε and α are the emissivity and absorptivity of the freeboard gas respectively and T the temperature. The previous relation is valid for the radiative heat transfer from gas to solids and walls.

To be shown next, the radiative heat transfer from the kiln internal walls to bed given by [35]:

$$Q_{radiation,w\to s} = \sigma A_{w\to s}\varepsilon_s\varepsilon_w\Omega\left(T_w^4 - T_s^4\right) \quad [W], \tag{3-4}$$

where Ω is the form factor for radiation which is calculated as follows [35]:

$$\Omega = \frac{L_{crd}}{2(\pi - \xi)R} \quad [-], \tag{3-5}$$

where L_{crd} is the length of the chord from the sector covered by the bed, ξ the dynamic angle of repose and R the kiln inner radius. This radiation model is limited to radiation heat transfer from the uncovered wall to the solids bed and from the freeboard to the exposed solids bed.

Lastly, the radiative heat losses from the shell to the environment follow the Stefan Boltzmann Law:

$$Q_{radiation,shell\to ambient} = \sigma A_{w\to s}\varepsilon_{shell}\left(T_{shell}^4 - T_{amb}^4\right) \quad [W], \tag{3-6}$$

where ε_{shell} is the emissivity of the outer shell and T_{shell} the surface shell temperature.

3-3 Convective Heat Transfer

There are various correlations for the convective heat transfer from the gas to solids. The selected correlations appear on recent publications for one dimensional models for Portland Cement Kilns [35, 29]. The following convective heat transfer coefficient correlation is used by Mujumdar and Li on their respective one dimensional Portland Cement Kiln models [35, 29]:

$$h_{g\to s}^c = 0.46\frac{k_g}{D_{eq}}\mathrm{Re}_g^{0.535}\mathrm{Re}_\omega^{0.104}\eta^{-0.341} \quad [W\cdot m^{-2}K^{-1}], \tag{3-7}$$

where k_g is the gas thermal conductivity and η the kiln load. Re_g and Re_ω are the gas phase and angular Reynolds numbers given by:

$$\mathrm{Re}_g = \frac{u_g D_{eq}}{\nu_g} \quad [-], \tag{3-8}$$

$$\mathrm{Re}_\omega = \frac{\omega {D_{eq}}^2}{\nu_g} \quad [-], \tag{3-9}$$

where u_g is the gas velocity, ν_g the kinematic viscosity of gas and ω the kiln rotational speed ($[rad/s]$). D_{eq} represents the equivalent diameter of the kiln given by [29]:

$$D_{eq} = \frac{0.5D(2\pi - \theta + \sin\theta)}{(\pi - (\theta/2) + \sin(\theta/2))} \quad [m], \tag{3-10}$$

where D is the internal kiln diameter and θ is the cross-sectional half angle due to the kiln fill as shown in Figure 1-2.

Similarly, the convective heat transfer coefficient from gas to internal walls is calculated by [35, 29]:

$$h^c_{g\to w} = 1.54\frac{k_g}{D_{eq}}\mathrm{Re}_g^{0.575}\mathrm{Re}_\omega^{-0.292} \quad [W\cdot m^{-2}K^{-1}], \tag{3-11}$$

which has the same nomenclature as Equation 3-7.

The previously presented heat transfer coefficient correlation was developed by Tscheng and Watkinson [6] experimentally and validated with data from the available literature.

Finally one defines the convective heat transfer coefficient between the outer wall and environment when $Re_w/\sqrt{Gr} \geq 0.2$ as [29]:

$$h^c_{sh\to a} = \frac{k_a \mathrm{Pr}^{0.3}}{D}\Big(\mathrm{Re}_a^2 + 0.5\mathrm{Re}_\omega^2 + Gr\Big)^{0.35} \quad [W\cdot m^{-2}K^{-1}], \tag{3-12}$$

where k_a is the thermal conductivity of the air, Pr is the Prandtl number, D is the outer diameter of the kiln, Re_a the Reynolds number of the ambient air, Re_ω the rotational Reynolds number and Gr the Grashof number given by:

$$Gr = \frac{g\beta(T_{shell} - T_{amb})D^3}{\nu^2} \quad [-], \tag{3-13}$$

where g is the acceleration due to gravity, β the volumetric thermal expansion coefficient from air, T_{shell} the shell surface temperature, ν the kinematic viscosity of air and D the outer diameter of the kiln.

Similarly, one has for $Re_w/\sqrt{Gr} < 0.2$ [29]:

$$h^c_{sh\to a} = \frac{k_a Pr^{0.3}}{D} C Re_a^N, \tag{3-14}$$

where N is the revolutions per minute and C a correction factor, which in the present case it is varied to adjust the heat transfer coefficient to match the experimental values from the plant and calibrate the model.

3-4 Wall to Bed Heat Transfer

As Boateng and Li remark on their publications [6, 29] there are a number of correlations for the wall to bed heat transfer coefficients. Due to this fact, two different correlations can be used in the model, from Boateng and Li [6, 29]. Both are based from modified penetration models that come from gas-solid fluidised bed reactors.

First, the correlation described by Boateng [6] is presented:

$$Nu = 11.6Pe^{0.3} \quad [-], \tag{3-15}$$

where Nu and Pe are the Nusselt and Peclet dimensionless numbers respectively given by:

$$Nu = \frac{h_{w\to s}R\xi}{k_b} \quad [-], \tag{3-16}$$

$$Pe = \frac{R^2\xi\omega}{\alpha_b} \quad [-], \tag{3-17}$$

where R is the kiln radius, ξ the dynamic angle of repose, ω the kiln rotational speed, k_b the thermal conductivity of the bulk solids and α_b the thermal diffusivity of the bulk solids.

This correlation takes into account the kiln rotational speed which is an operating parameter of the Kiln.

Secondly, the heat transfer coefficient developed by Li [29] is presented:

$$h_{w\to s} = \left(\frac{\chi d_p}{k_g} + \frac{0.5}{\sqrt{2k_b\rho_b c_{pb}n/\phi}}\right)^{-1} \quad [W\cdot m^{-2}K^{-1}], \tag{3-18}$$

where d_p denotes the particle diameter, k_g the thermal conductivity of the gas, k_b the thermal conductivity of the bulk solids, ρ_b the bulk density, $c_{p,b}$ the heat capacity of the bulk solids, n the r.p.m. of the kiln and ϕ the central half angle. Additionally, χ can take a value between 0.096 - 0.198 and denotes the thickness of the gas layer between the solids and the wall. This correlation has been validated with data from industrial Portland Cement Kilns and pilot-scale kiln data from literature [29].

3-5 Material Physical Properties

The physical properties for the gas and solids are calculated with existing correlations reported in literature [6, 29, 35]. However, for the bulk solids one has to take into account the void fraction of the material by averaging the solid and gas properties as follows:

$$\Phi_{eff} = e\Phi_{gas} + (1-e)\Phi_{solid} \quad [-], \tag{3-19}$$

where Φ corresponds to the physical property i.e., conductivity, emissivity, and so on, and e corresponds to the solid void fraction.

For the thermal conductivity and diffusivity of the bulk solids one uses the following expressions presented by Boateng which takes radiation into account [6]:

$$k_b = \frac{1-e}{\frac{1}{k_s}+\frac{1}{4\sigma\varepsilon d_p T^3}} + e4\sigma\varepsilon d_p T^3 \quad [W\cdot m^{-1}K^{-1}], \tag{3-20}$$

$$\alpha_b = \frac{k_b}{\rho_b c_{p,s}} \quad [m^2\cdot s^{-1}], \tag{3-21}$$

where e is the void fraction, k_s the thermal conductivity of the solids, σ the Stefan Boltzmann constant, ε the emissivity of the solids, d_p the diameter of the particles, T the temperature of the bulk solids, ρ_b the density of the bulk solids, $c_{p,s}$ the specific heat of the bulk solids and α_b the thermal diffusivity of the bulk solids.

It is important to note that most physical properties like heat capacity, density, conductivity and so on, are dependent on the temperature. The expressions for such properties can be found in literature.

3-6 Governing Equations: Heat Balances

By substituting the heat transfer paths from Chapter 1 into Equation 3-2 the heat balance of the bulk solids reads as follows:

$$\dot{m}_s c_{p,s}\frac{dT_s}{dz} = \frac{1}{L_K}\left[Q_{radiation,g\to s} + Q_{radiation,w\to s} + Q_{convection,g\to s} + Q_{conduction,w\to s}\right],$$

where by substituting in the right hand side the heat transfer paths with the correlations developed in the previous sections one gets,

$$\dot{m}_s c_{p,s}\frac{dT_s}{dz} = \frac{1}{L_K}[\sigma A_{g\to s}(\varepsilon_s+1)\left(\frac{\varepsilon_g T_g^4 - \alpha_g T_s^4}{2}\right) + \sigma A_{w\to s}\varepsilon_s\varepsilon_w\Omega\left(T_w^4 - T_s^4\right) + h_{g\to s}A_{g\to s}(T_g - T_s) + h_{w\to s}A_{w\to s}(T_w - T_s)], \quad [Js^{-1}m^{-1}] \tag{3-22}$$

where in addition to the nomenclature described in the previous sections one has T denoting temperature, A area of heat exchange and the subscripts s, g, and w denoting the bulk solids, gas and wall respectively. One can observe that the temperature of the gas is an input from a freeboard model or experimental data, thus the only unknowns of Equation 3-22 are the solids and wall temperature, T_s and T_w.

One then needs an additional equation due to the two unknown temperatures, T_s and T_w. Then by solving the energy balance across the kiln walls one gets:

$$Q_{gas\rightarrow wall} + Q_{radiation,gas\rightarrow wall} - Q_{wall\rightarrow solids} - Q_{radiation,wall\rightarrow solids} = Q_{shell\rightarrow ambient} \quad [W]. \tag{3-23}$$

Then by substituting one obtains:

$$h_{g\rightarrow w}A_{g\rightarrow w}(T_g - T_w) + \sigma A_{g\rightarrow w}(\varepsilon_w + 1)\left(\frac{\varepsilon_g T_g^4 - \alpha_g T_w^4}{2}\right) - h_{w\rightarrow s}A_{w\rightarrow s}(T_w - T_s) - \sigma A_{w\rightarrow s}\varepsilon_s\varepsilon_w\Omega\left(T_w^4 - T_s^4\right) = Q_{shell\rightarrow ambient} \quad [W], \tag{3-24}$$

where $Q_{shell\rightarrow ambient}$ denotes the heat losses from the shell of the kiln to the environment. Then by using Newton's law of cooling one obtains the following:

$$Q_{shell\rightarrow ambient} = UA_{shell}(T_w - T_{amb}) \quad [W], \tag{3-25}$$

where A_{shell} is the outer area of the steel shell of the kiln, T_w is inner wall temperature, T_{amb} the ambient temperature and U_{shell} is the overall heat transfer coefficient given by [4]:

$$U_{shell} = \frac{1}{\frac{\log(R_{lin}/R_{in})}{k_{lin}2\pi L} + \frac{\log(R_{out}/R_{lin})}{k_{steel}2\pi L} + \frac{1}{h^c_{sh\rightarrow amb}}} \quad [W \cdot m^{-2}K^{-1}], \tag{3-26}$$

where R is the radius, k the thermal conductivity, L the length of the section and $h^c_{sh\rightarrow amb}$ the convective heat transfer coefficient between the kiln outer wall and the environment and the subscripts *in*, *out*, *lin* denote inner, outer and lining respectively.

It is to be noted that Equations 3-22 and 3-24 encompass a differential algebraic system of equations where one solves for T_s and T_w, where the initial values come from in-field measurements.

3-7 Chemical Reactions and Clinker Melt Model

The reactions occurring in the kiln are of the following form:

$$\gamma CaO(s) + \alpha Al_2O_3(s) \rightarrow \gamma CaO \cdot \alpha Al_2O_3(s). \tag{3-27}$$

Given available XRD (X-Ray Diffraction) data for a 2:3 molar ratio of CaO and Al_2O_3[1], and using data such as the activation energy present in literature, a simplified reaction model taking only into account the conversion of Alumina will be developed.

One can describe the rate of a solid-state reaction by the following Arrhenius type equation [24]:

$$\frac{d\alpha}{dt} = A_P e^{-(E_a/RT)} f(\alpha), \tag{3-28}$$

where A_P is the pre-exponential factor, E_a the activation energy, T the absolute temperature, R the universal gas constant, $f(\alpha)$ the reaction model, t is time and α the conversion fraction.

One starts by selecting a diffusion reaction model. Due to the sintering of Lime and Alumina being controlled by diffusion [20, 34], we select the Ginstling-Brounshtein (D4) model which is given for the differential form in Equation 3-28 [24] as:

$$D_4(\alpha) = f(\alpha) = 3\Big[2((1-\alpha)^{-1/3} - 1)\Big]^{-1}, \tag{3-29}$$

where α is the conversion fraction as in Equation 3-28. This reaction model was developed for diffusion controlled reactions in three dimensions.

It is to be noted that the experimental data available is non-isothermal, thus one makes use of the heating rate which is also available and one has:

$$\frac{d\alpha}{dT} = \frac{A_P}{\beta} e^{-(E_a/RT)} f(\alpha), \tag{3-30}$$

where β is the heating rate (dT/dt).

By selecting an activation energy of $E_a = 205$ kJ/mol we then proceed to adjust Equation 3-30 by varying the pre-exponential factor A_P. This activation energy value corresponds to $Ca \cdot Al_2O_3$ [34], which is the primary component for the product manufactured at the plant to be analysed. By iterating and taking the best fit, the exponential factor has the value $A = 14500\ s^{-1}$.

It is to be noted that the simplified model is only for the conversion of Alumina, it does not take into account side reactions and intermediates which are known to occur. The previous model is valid only for feed rates of 2:3 molar ratio of CaO and Al_2O_3 with operating temperatures from 1173 to 1973 degrees Kelvin.

We then modify Equation 3-22 and include the heat of reaction (ΔH^{rxn}):

[1] XRD data from Industrial Partner

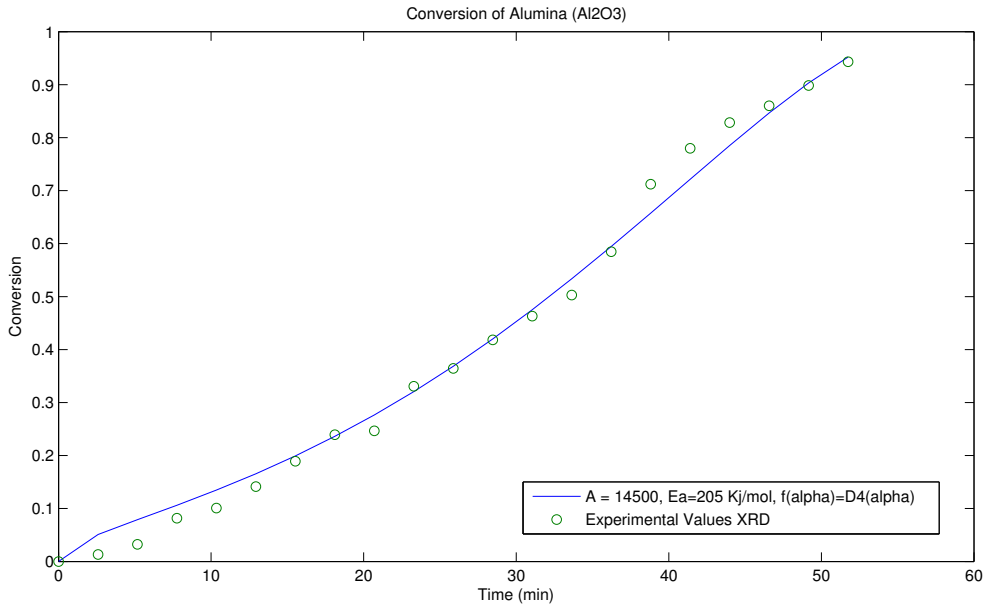

Figure 3-2: Conversion of Alumina vs. Time chart, $R^2 = 0.997$

$$\dot{m}_s c_{p,s} \frac{dT_s}{dz} = Q_{radiation,g\to s} + Q_{radiation,w\to s} + Q_{convection,g\to s} + Q_{conduction,w\to s} + \dot{n}_{Al_2O_3} \Delta H^{rxn}, \tag{3-31}$$

where $\dot{n}_{Al_2O_3}$ is the moles of Al_2O_3 consumed per unit length ($dn_{Al_2O_3}/dz$).

One defines the heat of reaction as $\Delta H^{rxn} = 30$ kJ/mol which is an average between the heat of reaction of $Ca \cdot Al_2O_3$ (31 kJ/mol) and $Ca \cdot 2Al_2O_3$ (29 kJ/mol), the main components of the kiln products. One then need to solve the following:

$$\frac{\mathrm{dn}_{Al_2O_3}}{dz} = x_{Al_2O_3,0} \frac{\dot{m}_s}{Mw_{Al_2O_3}} \frac{\bar{\tau}}{L_K} \frac{d\alpha}{dt} = x_{Al_2O_3,0} \frac{\dot{m}_s}{Mw_{Al_2O_3}} \frac{\bar{\tau}}{L_K} A_P e^{-(E_a/RT)} D_4(\alpha), \tag{3-32}$$

where $x_{Al_2O_3,0}$ is the molar fraction at the feed of the kiln, $\dot{m}_s$ the mass flow of the solids, $Mw_{Al_2O_3}$ the molecular weight of Alumina, $\bar{\tau}$ the residence time of the kiln and L_K the length of the kiln.

For the clinker melt model the following relationship presented by Mujumdar [35] is used:

$$\mathrm{m}_L = \max\left[0, \frac{T_s - T_{solidus}}{T_{liquidus} - T_{solidus}}\right], \tag{3-33}$$

where m_L is the fraction of the bed which is in liquid phase, T_s the bulk solids temperature, $T_{solidus}$ the solidus temperature of the material bed and $T_{liquidus}$ the liquidus temperature of the bed.

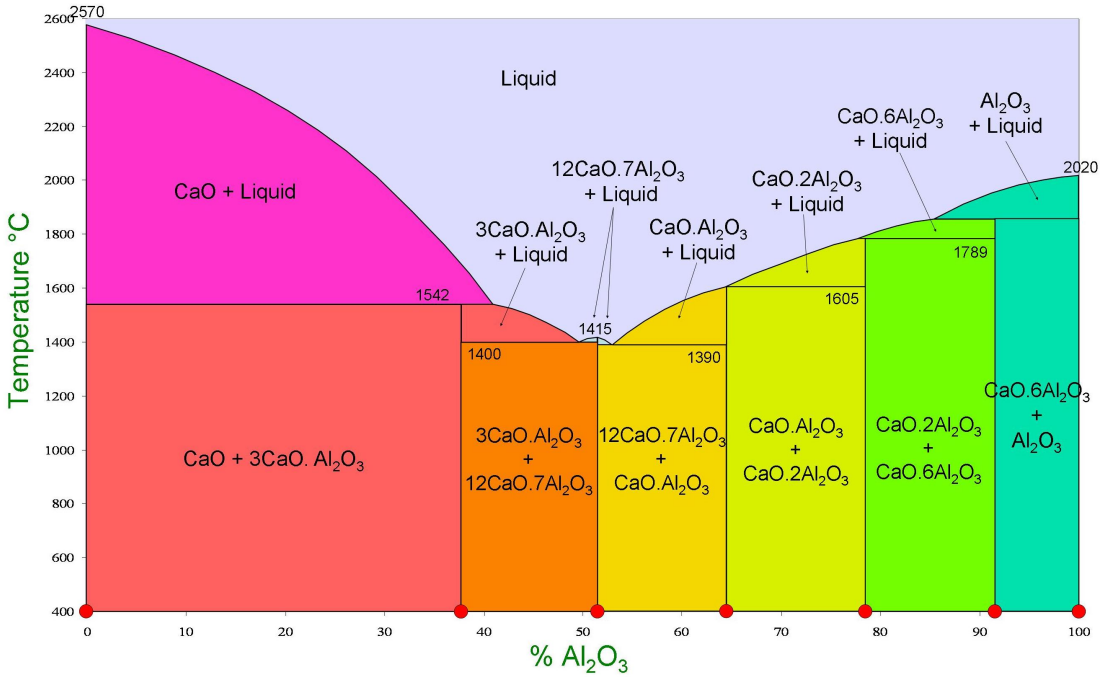

Figure 3-3: Phase Diagram for Calcium Aluminates

One then selects 2570^{o}C and 1390^{o}C as liquidus and solidus temperatures respectively. It can be observed in Figure 3-3 that the selected liquidus and solidus are the limit temperatures for Calcium Aluminates. It is known that the method may not be exact, as mass fractions for the different phases for the calcium aluminates are not known, but it is a method which brings qualitative results into perspective. In further work, where a full study on chemical kinetics is done, a full clinker melt model can be developed to deliver quantitative results.

By solving Equation 3-33, 3-32 and 3-24 simultaneously, one can get the temperature profile of the bed and wall, the conversion of Alumina and the melt fraction.

3-8 Solution Procedure

First, the temperature field calculated from the freeboard CFD model was processed to have a 1-D average freeboard gas temperature. Then one runs the ODE model taking the temperature of the solids at the feed of the kiln as an initial condition.

The system described by solving Equations 3-22, 3-25 and 3-32 is a differential algebraic equation system. For initial values one defines the composition and temperature at the feed position of the kiln. The described initial values are operating parameters which are usually known.

An implementation in MATLAB [33] was done by using the ODE and DAE solver "ode15s" for Equations 3-22, 3-25 and 3-32 to solve for T_s, T_w and $\dot{n}_{Al_2O_3}$.

The mentioned solver is based on numerical differentiation formulas, which were developed to integrate stiff ordinary differential equations of the following form:

$$y' = F(t, y), \tag{3-34}$$

and

$$M(t)y' = f(t, y), \tag{3-35}$$

where $M(t)$ is a mass matrix that is usually sparse and t denotes time. One refers to the documentation from MATLAB for more information on the numerical method used [33].

After solving the DAE system, one then uses the solution from Equation 3-22 to solve Equation 3-33 and get the melt fraction m_L.

3-9 Validation

To validate the model, experimental work from Barr et al. was used [3]. The paper from Barr aims to provide pilot kiln data for the verification of heat-transfer models. It considers experiments with an inert bed and with calcination reactions. Run T4 from the mentioned paper was used due to the fact that it is an experiment with an inert bed. The geometry and operating conditions of the kiln used for the experimental work from Barr are described in Table 3-1.

Geometry		Operating Conditions		Properties	
L_K	5.5 (m)	n	1.5 (rpm)	k_b	0.27 (W/m k)
D_K	0.406 (m)	$\dot{m}_s$	17 (g/s)	ρ_s	1650 (kg/m^3)
η	12% (-)	U_g	2 (m/s)		

Table 3-1: Data from Barr et al. [3] used in the 1-D model validation

In addition to the data described in the previous table, data from other one-dimensional models was used for the freeboard and lining [6, 29, 35]. In order to calibrate the model, the experimental results of the heat flux at the outer shell were matched with the results from the model by varying the outer shell convective heat transfer coefficient of the model. We can observe in Figure 3-4 the match obtained with respect to the heat flux at the outer shell.

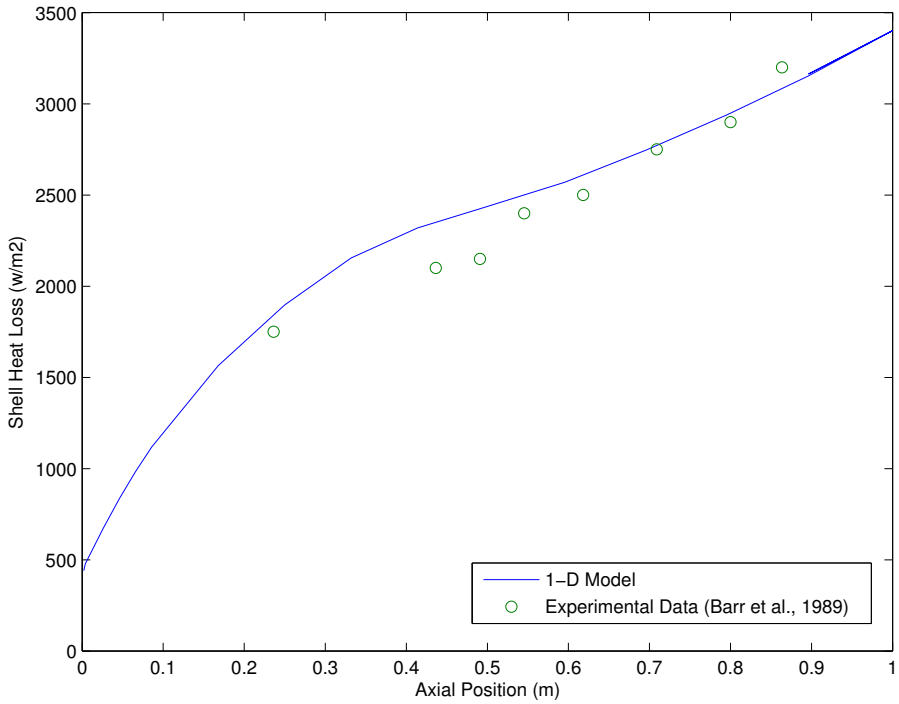

Figure 3-4: Outer Shell Heat Loss [3]

It can be observed in Figure 3-5 a clear matching between the developed 1-D model and the experimental results from Barr et al [3]. It is to be noted that the experiment run analysed was done without chemical reactions.

The previous results indicate that the model developed is valid for rotary kilns with an inert bed. Furthermore, it can be inferred that for the kiln to be analysed the model is also valid as reaction kinetics are derived and validated with experimental data.

However, in order to have a more rigorous validation with regard to chemical reactions an the possibility of the inclusion of a more exact model for clinker melt and scale formation on the lining, one would need experimental data with a pilot kiln using the Calcium Aluminates as feed and similar operating conditions to the kiln in question. One can refer to the experimental setup from Barr et al. and the pilot kiln used in his publication [3].

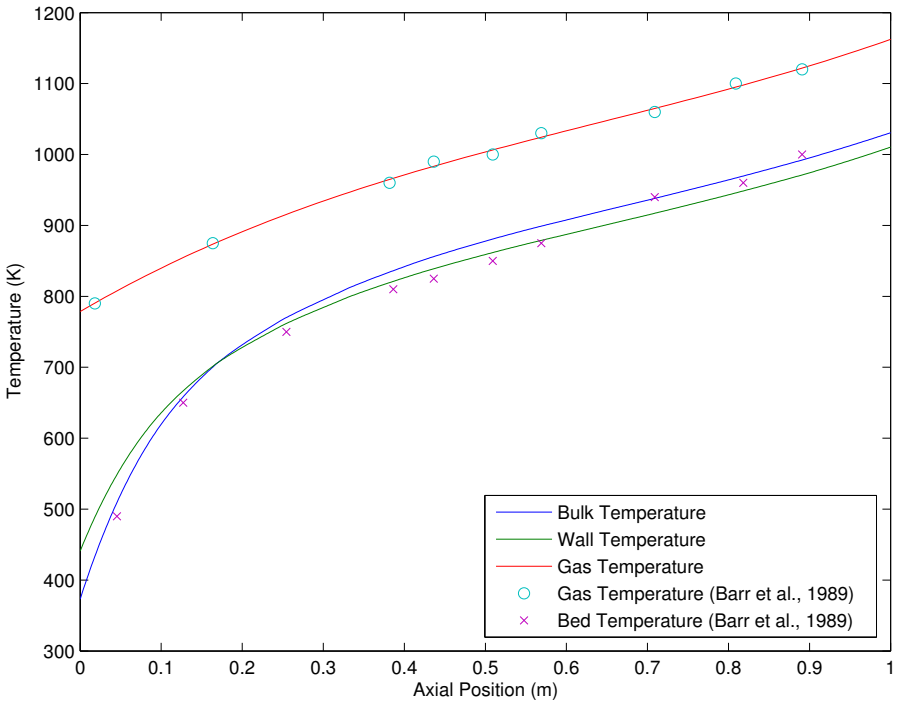

Figure 3-5: Temperature Profiles of the 1-D model and run T4 from Barr et al. [3]. Where in addition to the bulk solids temperature T_s, the wall temperature T_w and the gas temperature T_g, one can observe the gas and bed temperature experimental values.

.

3-10 Industrial Case Study: Air to Gas Ratio of 9 and 12

For the the present section, two cases (9 and 12 Air to Gas ratio) using the freeboard CFD model developed by Pisaroni [39] and data from the Industrial Plant are to be analysed with the previously described one-dimensional model.

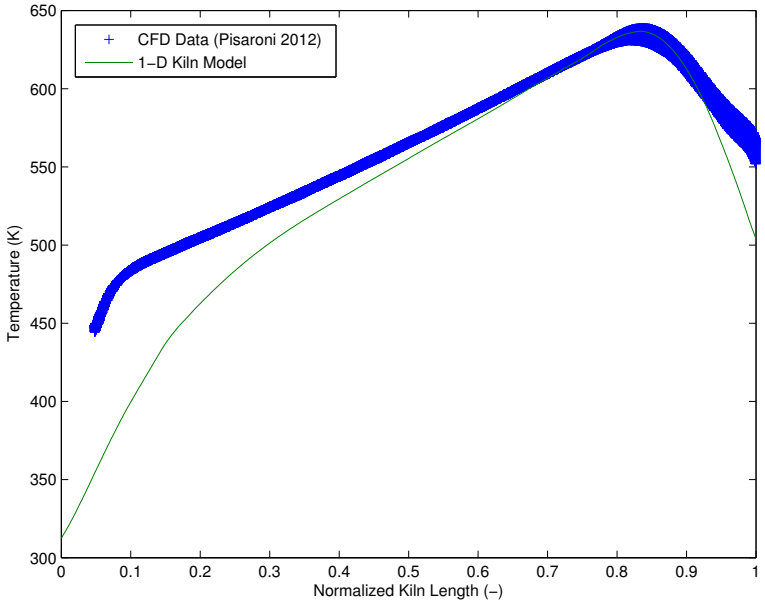

Figure 3-6: Outer Steel Shell Temperature from CFD Model and 1-D Model for 9 Air to Gas ratio [39]

In Figure 3-6 it can be observed the outer steel shell temperature profiles for the 1-D model and the CFD model. As the outer steel shell temperature is one of the few operating conditions that can be measured from the industrial plant, one varies the outer shell convective heat transfer coefficient to match the model with the data from the plant. The CFD data from the outer steel shell is validated using the same approach, hence we show the data from both models to show the validity of the approach. It is to be noted that the same approach was followed for the validation of the model on the previous section.

The Temperature Profiles are shown in Figure 3-7. One can observe that the peak temperature of the solids and the wall is around 2189 K and 2190 K respectively for the air to gas ratio of 9. This corresponds roughly to the wall temperature reported by Pisaroni from his freeboard CFD model for the kiln given as 2227 K [39]. It can be inferred that the temperature difference between the models is due to the solids present in the kiln. Similarly, for air to gas ratio of 12 one has a solids and wall temperature of 2105 K and 2110 K respectively compared to the CFD model wall temperature of 2167 K [39]. One can also observe that from kiln length 0.50 to 0.85 very similar temperatures from the wall and solids can be observed in both cases, a characteristic observed in the literature when validating results with experimental data where radiation is the main path for heat transfer [35, 29, 16].

While the overall trends of the model can seem appropriate, such as the rapid initial heating

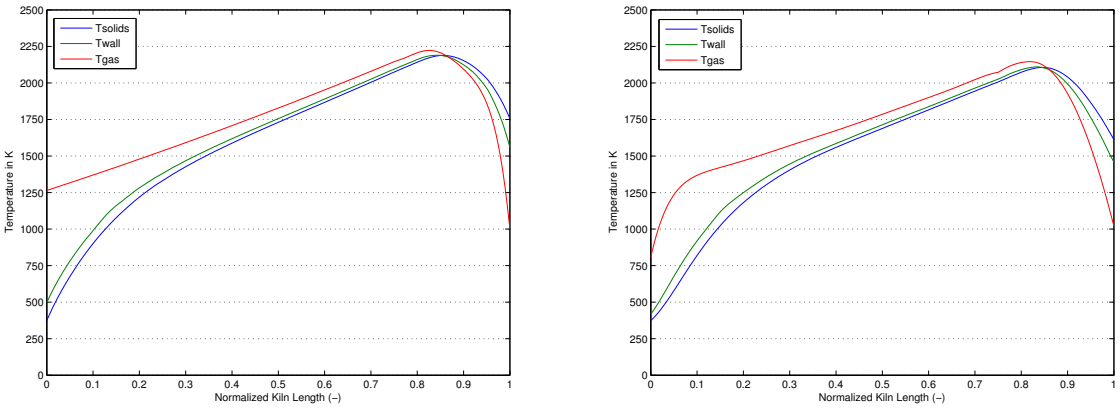

(a) Air to Gas Ratio: 9 (b) Air to Gas Ratio: 12

Figure 3-7: Temperature Profiles of 1-D Alumina Cement Kiln Model using CFD data [39]

of the solids [3], there are also shortcomings which can be appreciated at the discharge ends of both cases in Figure 3-7. The temperature of the bed material is significantly higher (at 1750 and 1625 K) than what is reported from the industrial plant. This could be due to the fact that there are inaccuracies in the CFD model near to the discharge end of the kiln[2]. It is to be noted the fact that the air temperature near the discharge end of the kiln can be used as a parameter to calibrate the kiln with data from the discharge from the plant.

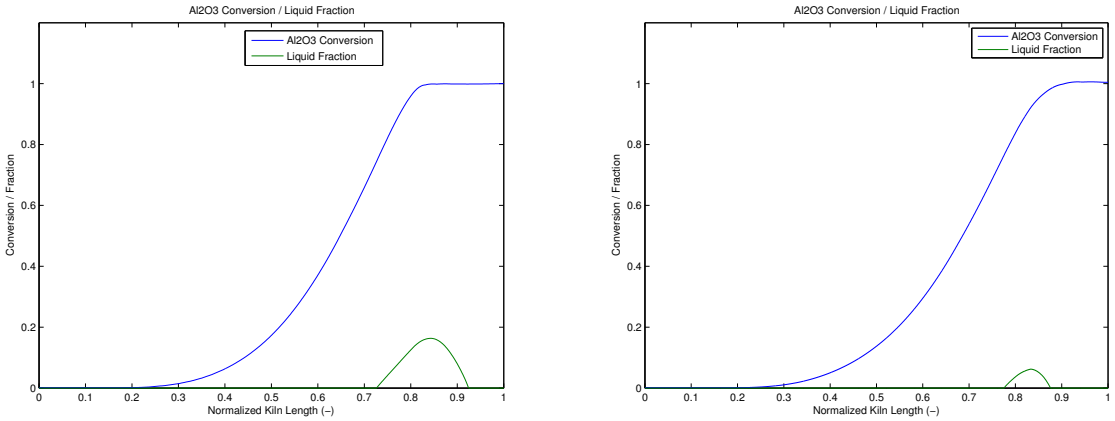

(a) Air to Gas Ratio: 9 (b) Air to Gas Ratio: 12

Figure 3-8: Conversion of Alumina and Liquid Phase Fraction [39]

It can be observed in Figure 3-8a that at 80% of the the kiln length the conversion of Alumina is complete. The reaction kinetics available does not account for what happens after the conversion is complete, thus the kiln modelled could have side reactions that occur after the Alumina has been completely consumed. This is in contrast to Figure 3-8b where full conver-

[2]Personal Communication with Michele Pisaroni, 2012

sion is attained at 90% of the kiln. As full conversion is achieved closer to the discharge end of the kiln, the possibility of side reactions after the Alumina has completely been consumed is decreased with a air to gas ratio of 12.

One can also observe in Figure 3-8 an estimate of the melt fraction. This indicates that the highest amount of melt is near the peak temperature position of the kiln. This is in agreement to the location of the temperature and incident radiation peaks from the CFD simulations from Pisaroni [39]. Additionally, it can be observed that the liquid fraction in the air to gas ratio of 12 is lower than in the air to gas ratio 9 case. This also corresponds to operating conditions observed in the kiln where ring formation was minimised with the air to gas ratio of 12.

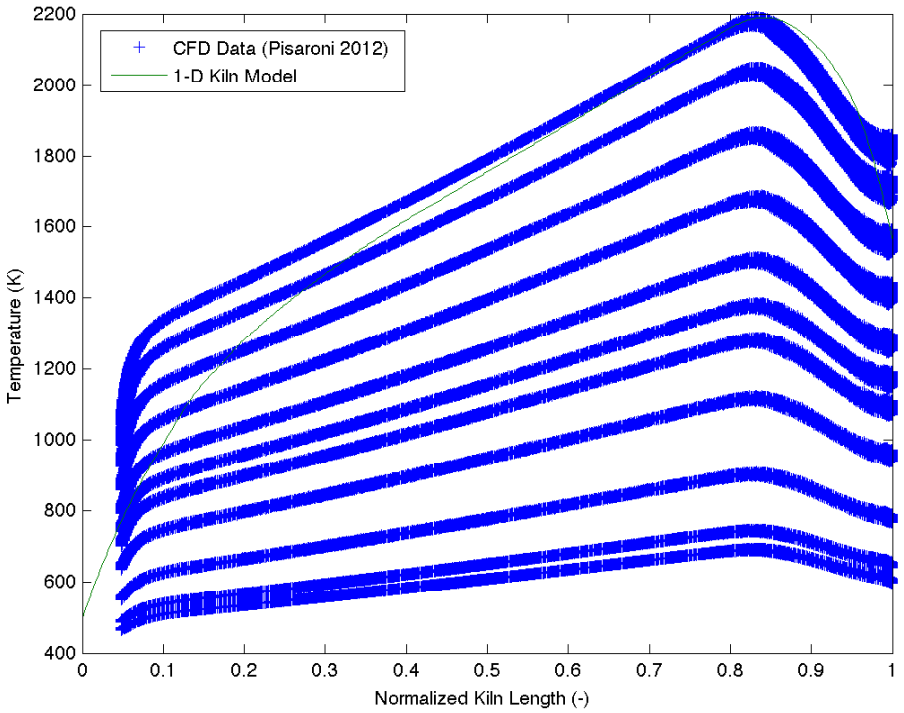

Figure 3-9: Lining Temperature from CFD Model and 1-D Model for 9 Air to Gas ratio [39]

For Figure 3-9 it can be observed that the peak temperature of lining from the 1-D model corresponds with the data from the CFD model. This shows that the simplified radiation model previously presented is indeed valid for the kiln model presented. It is to be noted that the various thick curves from the CFD data in the figure indicate different lining position. The top CFD data curve indicates the lining surface temperature, denoted in the model as wall temperature.

One should note that the CFD freeboard model overestimates the gas temperature[3]. This is probably the reason for the high operating temperatures of the solids observed in the 1-D model results.

[3]M. Pisaroni. Personal Communication 2012

3-11 Conclusions

From this section one can draw the conclusion that the one-dimensional model can give reliable results only if there is well-founded information about the freeboard. The temperature profile from the gases could come from experimental data or freeboard models such as the CFD freeboard model used in the industrial case study.

Therefore, it is reasonable to assume that due to the inconsistencies of the CFD freeboard model in certain areas of the kiln[6] and the lack of reliable in-field data, the results presented from the Industrial case study can only be interpreted as a qualitative guideline for kiln operation and design.

The one-dimensional kiln model can be used to explain the consequences of doing changes on the air to gas ratio of the studied kiln, as it was shown in the previous section. It was also shown that the model is able to explain observed phenomena in the plant, such as product quality and ring formation position. Thus, it is proven that it could be used as a tool to explain and improve operation in a qualitative manner.

Chapter 4

Transversal Heat Transfer Model

In the present chapter a model for transversal heat transfer for the granular bed of the studied kiln will be developed taking as a basis the work from Boateng [6] and the following considerations:

- One uses the same correlations for heat transfer coefficients and physical properties as in Chapter 3,
- the granular material will be taken as a continuum for heat transfer purposes,
- the transversal model needs velocity fields from a granular flow model as input,
- due to a lack of experimental data for a granular flow model, the transversal model can be used only as a qualitative aid.

4-1 Governing Equations: Heat Balance

By considering a heat balance in a control volume in the transversal plane of the kiln one gets the following [6]:

$$\frac{\partial}{\partial x}\left(k_{eff}\frac{\partial T}{\partial x}\right)+\frac{\partial}{\partial y}\left(k_{eff}\frac{\partial T}{\partial y}\right)-\rho c_P u_x\frac{\partial T}{\partial x}-\rho c_P u_y\frac{\partial T}{\partial y}=-\frac{\dot{m}_s}{A_{AL}}c_P\frac{dT_{ax}}{dz}, \tag{4-1}$$

where k_{eff} is the effective conductivity as in Chapter 2, ρ the density, c_P the heat capacity, u the mean velocity components of the granular bed, $\dot{m}_s$ the mass flow and A_{AL} the active layer area. The first two terms of the left hand side represent the diffusive part of the heat equation, the third and fourth terms represent the advection due to movement of the bed and the right hand side is the temperature gradient in the axial direction due to the movement of the bed in axial direction. When taking into account a rolling bed, the right hand side term is equal to zero in the plug flow layer, as it is assumed that the axial movement of the bed occurs only in the active layer [6].

It can be observed that in Equation 4-1 one has all the input data from the 1-D model except for the velocity fields needed for the advective terms.

4-2 Velocity Fields

Due to the findings by using the DEM model in Chapter 2, one needs to generate a velocity field in order to use it with the proposed continuum transversal heat transfer model. Thus, a rolling bed velocity field was generated and imposed, Figure 1-4 denotes the described velocity field. While it is known that a typical active layer depth should typically be 10% of the bed height [6], due to the low bed height an overestimation of 20% active layer depth was generated in order to have more clear qualitative characteristics.

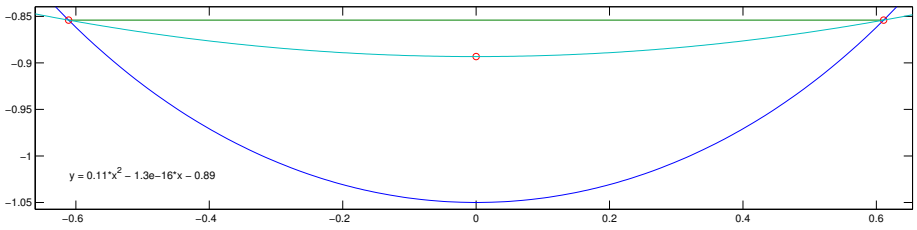

(a) Active and Passive Layer

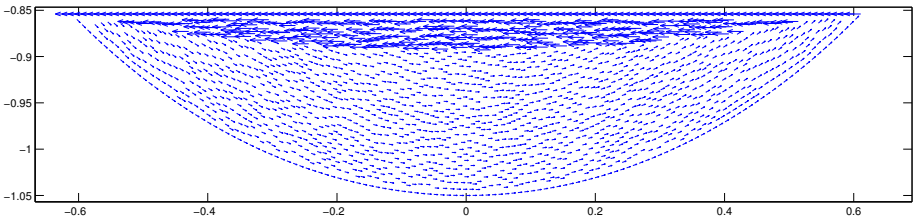

(b) Velocity Field

Figure 4-1: Generated Rolling Bed Velocity Field

In Figure 4-1a one can observe the generated active layer and passive layer. The curve in between the active and passive layers was generated via a quadratic regression. In Figure 4-1b the rolling bed velocity field can clearly be observed as described in Figure 1-4. The passive layer has a tangential velocity equal to the rotational speed of the kiln and the active layer has a rolling velocity proportional to the passive and active layer depth, i.e. 0.8/0.2 times the tangential velocity. This relationship is based on a material balance derived from the assumption that the material bed is to be taken as a continuum.

Note that Figure 4-1 is not equally scaled in the x and y axis.

4-3 Solution Procedure

For the solution procedure, an "Asynchronous solution of the one-dimensional and two-dimensional problem" is followed as described by Boateng [6].

With this approach, one first runs the 1-D model presented in Chapter 3 to get the temperature profiles, heat flux from the freeboard to the walls and bed and the temperature gradient along the axis of the kiln. One then uses this data as input for the transversal heat transfer model. As Boateng mentions [6], implicitly it is assumed that the heat transfer within the bed in the transverse plane does not alter the freeboard, bed and wall.

However, as in the present case only qualitative characteristics are considered, one uses the transversal heat transfer model independently from the one-dimensional model to bring insight on the need to characterise the granular flow of the bed.

One then proceeds to solve Equation 4-1 for the lining, bed and steel shell by using the Finite Element Method with the PDE Toolbox from MATLAB [33]. One can observe the computational domain and initial triangular unstructured mesh in Figure 4-2.

As boundary conditions, Neumann Boundary conditions are selected for the inner boundaries which represent the Heat Flux per unit length [W/m] from the freeboard gases to the material bed and kiln walls. It is to be noted that if reliable data on the velocity fields was given, the outer boundary would have been given as a Heat Flux to the exterior which would be varied to calibrate the model with the steel shell temperature. However, as the model is used qualitatively, the temperature is selected to be 500 K as Dirichlet boundary conditions.

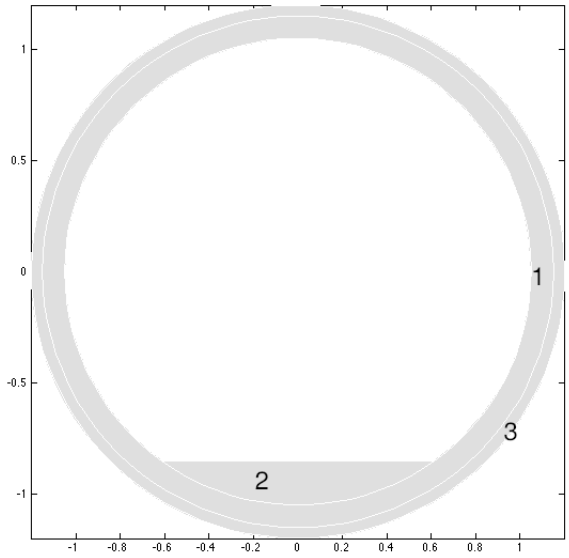

(a) Computational Domain: 1) Lining, 2) Granular Bed, 3) Steel Shell

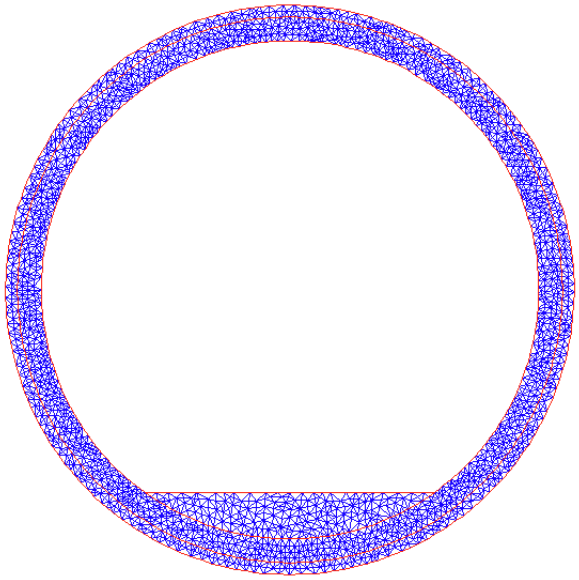

(b) Unstructured Mesh

Figure 4-2: Transversal Model: Geometry and Mesh

4-4 Results and Discussion

Experimental runs with varying inner boundary heat fluxes from 5000 to 17000 [W/m] and varying the transversal velocity fields were done. The Dirichlet outer boundary conditions were kept constant at 500 [K]. This methodology was followed in order to explore the effects the velocity fields have on the temperature profile of the transversal plane of the granular material from the kiln to be analysed.

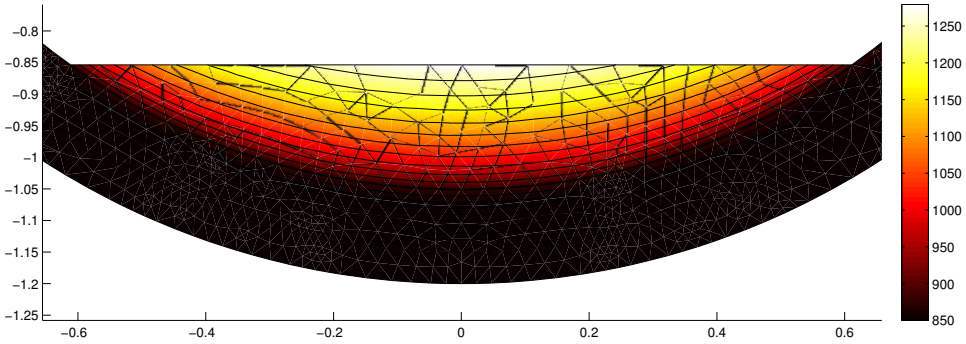

(a) Packed Bed

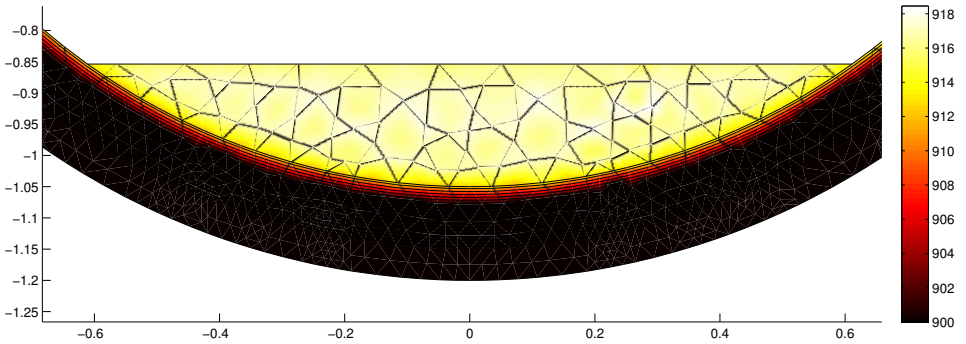

(b) Rolling Bed with 20% Active Layer

Figure 4-3: 2-D Transversal Model: 5000 W/m

It can be observed in Figures 4-3 to 4-6 the limit cases of having a packed and rolling bed. In all numerical experiments it was observed that having a rolling bed produces an uniform temperature on the granular material. A packed bed causes temperature profile which is undesirable for the operation of the kiln. Furthermore, at higher heat fluxes the temperature profile of either cases is much more uniform. This can be seen in Figure 4-3a, where the temperature difference within the bed is 400 K, Figure 4-4a where the difference is 300 K, Figure 4-5a 250 K and Figure 4-6a 200 K. As the freeboard heat flux is dependent on the freeboard gas temperature, the results indicate that at higher operating temperatures the granular bed temperature profile is more uniform than at lower temperatures. Intuitively, this is due to the effective conductivity on the granular bed which takes into account radiation effects, refer to Equation 3-20.

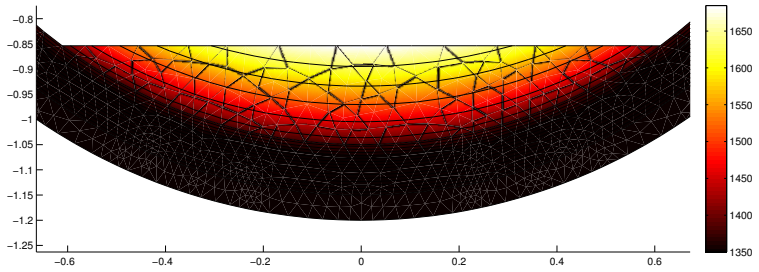

(a) Packed Bed

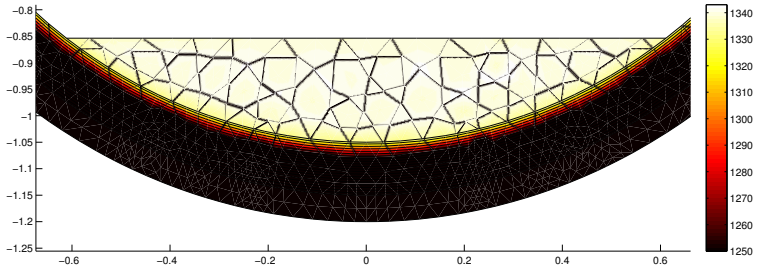

(b) Rolling Bed with 20% Active Layer

Figure 4-4: 2-D Transversal Model: 10000 W/m

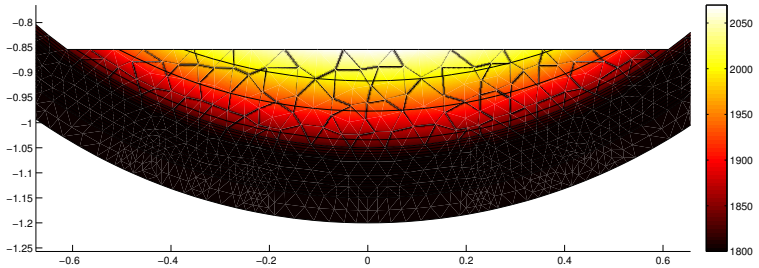

(a) Packed Bed

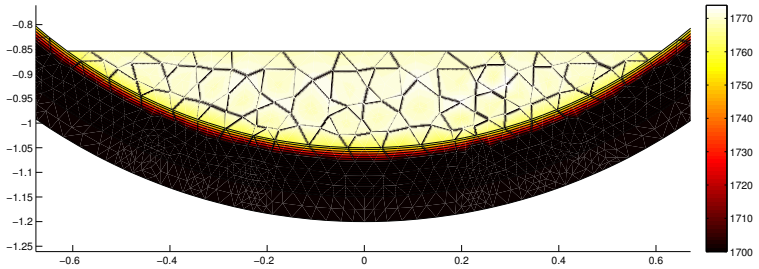

(b) Rolling Bed with 20% Active Layer

Figure 4-5: 2-D Transversal Model: 15000 W/m

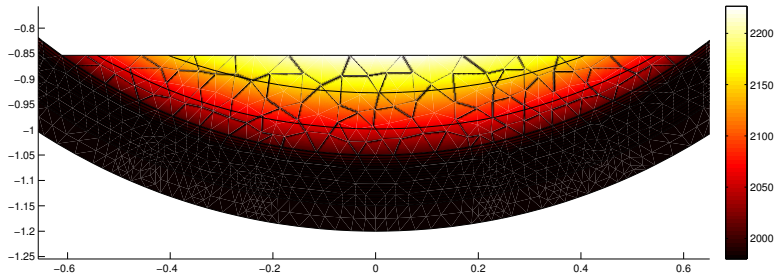

(a) Packed Bed

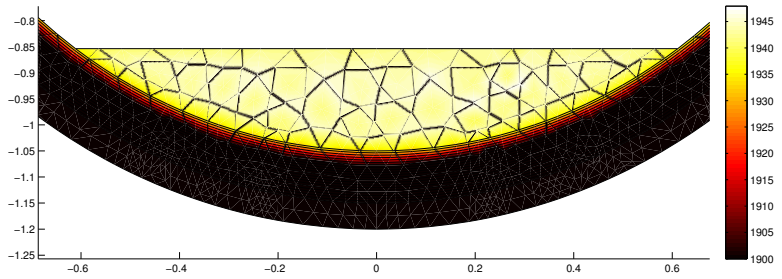

(b) Rolling Bed with 20% Active Layer

Figure 4-6: 2-D Transversal Model: 17000 W/m

It was then proceeded to select a bed height of 20% and imposed the velocity for the particles rolling back in the active layer with the same velocity magnitude as the plug flow layer. It can be observed on Figure 4-7 that the effect of this that around 70% of the granular bed cross-section is of uniform temperature, with the total temperature difference in the bed of 80 K.

It can then be concluded that even though the kiln has a low loading of 5%, the effects of the transversal granular velocity fields are important for the detailed modelling of the rotary kiln. One then can infer that there is a need to characterise the mixing of the granular bed in order to translate this into a velocity field that can be used in the continuum transversal heat transfer kiln model.

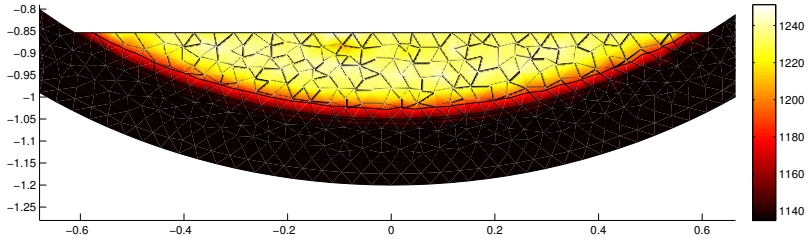

Figure 4-7: 2-D Transversal Model: Plug Flow Velocity Field

4-5 Conclusions

One can conclude from the previous experiments that due to the low loading and high temperatures of the kiln, one not needs a perfect rolling bed regime to have an uniform transversal temperature on the granular bed of the kiln. However, considering the results of the previous sections one cannot conclude whether the transversal granular flow can be neglected or not for heat transfer purposes.

The experiments show that if the kiln in question is operating in a rolling bed mode with an active layer of 5% to 20%, the temperature profile in the transversal plane of the bed is uniform.

In order to draw more detailed conclusions with this respect, further research must be done to be able to characterise the transversal flow of the analysed kiln.

Considering that temperature uniformity is directly proportional to product uniformity, the need for a characterisation of the transversal flow of the industrial kiln is highlighted. If further work is conducted in order to characterise the transversal flow, the benefits for the industrial partner would be with regard to the improvement of mixing for further kiln designs, which could be translated into better product quality.

Chapter 5

Conclusions

5-1 Transversal Flow Modelling

As shown in Chapters 2, 3 and 4, it is clear that there is a need for the characterisation of the transversal flow of the kiln in question. This would bring important knowledge with regard to operating conditions and modelling guidelines.

As it was seen in Chapter 2, there is no clear indication that the operating granular flow regime is a rolling bed. Thus, there could be opportunity areas for the design and operation of CAC kilns based on the studied kiln due to non-optimised mixing in the granular bed.

From a modelling perspective, if the kiln is operating in a rolling regime, then the one-dimensional model would suffice for the design and improvement of operating capabilities of the CAC kiln in question as the model could be used quantitively if there is a reliable freeboard model or experimental data. This is in contrast to not having a rolling regime, which in turn can be translated into a qualitative use of the one-dimensional granular bed model.

Additionally, a transversal heat transfer continuum approach would be possible only with steady state velocity fields in the granular material or a steady state characterisation of the different operating modes. However, if the regime is other than rolling, the transversal heat transfer approach presented on the present work would not be possible as it relies on steady state velocity fields.

Thus, it is to be stressed the importance of experimental data in order to explore the transversal flow mode of the kiln and take pertinent decisions, on a practical and a modelling perspective.

5-2 One-dimensional Kiln Bed Model

A one-dimensional kiln bed model is an adequate tool to show qualitative bulk solid properties from the Calcium Aluminate Cement (CAC) Kiln in question. Thus it can be used as an aid

in sensitivity analysis for the suggestion of operation and design changes of the kiln.

By having the industrial case study and being able to explain and draw conclusions based on CFD data and observed behaviour at the plant, it was shown that the model is indeed valuable for qualitative analysis of the studied rotary kiln.

One must note that there are opportunity areas for the one-dimensional model. The first can be seen as the dependancy to reliable freeboard data. Secondly, the need for more complete reaction kinetics would not only bring insight on the concentration profiles of the different components of the granular bed, but also more exact estimations of clinker melt as the different Calcium Aluminates phases have different liquidus and solidus temperatures. Finally, if one takes into account the kiln lining surface scale one could have more exact heat transfer phenomena in the kiln due to the fact that the scale would be an extra thermal resistance for the heat shell losses.

5-3 Transversal Heat Transfer

The study done on the transversal heat transfer of the rotary kiln from the industrial partner shows that due to the low loading and high temperatures, one does not need to have a rolling bed in order to have a near uniform temperature profile. It also shows that by having a rolling mode with an active layer of 5% - 20% one has a uniform temperature profile.

However, due to the previously described shortcomings on the transversal flow characterisation, neither a quantitative nor a qualitative use of the transversal model can be done. This is due to the dependency of the transversal heat transfer model to the granular bed transversal velocity fields.

Thus, the main shortcoming of the mentioned model is the dependency of reliable steady state flow fields. Hence, there is an area of opportunity to either develop a correlation that captures the characterisation of the transversal flow mode into 2-D continuum model, or to fully develop a DEM model taking into account all heat transfer paths, sintering, cohesion, and so on.

5-4 Concluding Remarks

One can conclude that the approach followed in the present work not only brings suggestions of guidelines for the operation and design of CAC kilns, but remarks the need for further work in order to have more exact quantitative models and guidelines for CAC rotary kilns.

In the next chapters, specific recommendations for industrial partner and an outline for further work will be addressed.

Chapter 6

Recommendations

From the work presented a series of recommendations will be done for the improvement of operation and design of the kiln in question.

6-1 Rotary Kiln Sensitivity Analysis

First point is to undergo a sensitivity analysis to explore the effects of different values for the kiln design variables such as, length, diameter, load and rotational speed. The objective of doing so is for the potential maximisation of production and minimisation of energy consumption.

This can be done with the one-dimensional model in hand if there is a more exact freeboard model available. While it is known that there is ongoing work for the implementation of a more exact combustion model for the Freeboard model by Pisaroni [39], it is still uncertain to what extent the results are more representative than the ones presented in his work from 2012 [39].

It is imperative to develop a one-dimensional freeboard kiln model in order to have fast results while varying the kiln design variables. However, when having results from the described 1-D Kiln model one needs to run a more detailed model in order to confirm its results for use in the design or scale-up of CAC Kilns.

Implicit is the need of validated one-dimensional and three-dimensional kiln models for its use in design and scale-up.

6-2 Environmental Variables

Secondly, it is important to take into account the environmental conditions when designing and selecting the location for rotary kilns. This is due to the potential unsteady heat losses and the difficulty for its analysis.

By taking as an example the current work, one can remark the difficulty of gathering data from the analysed kiln due to environmental conditions present at the plant from the industrial partner. However, one should also analyse the impact these environmental conditions have on the energy efficiency, product quality and control of the kiln.

6-3 Pilot Kiln for Experimental Trials

Third and most importantly, a research scale pilot kiln would be a wise investment in order to develop better models for the design and operation philosophies for future kilns.

It was remarked previously the need of a sensitivity analysis with experimentally validated numerical models. A pilot kiln can be used for the validation and development of mentioned models. One can have a similar set up as Barr had for his experiments [3]. With the mentioned set up it would be possible to validate both, a freeboard model and a granular bed model.

In addition to this, the transversal granular flow mode can also be explored with the pilot installation. As remarked earlier, characterisation of transversal flow is also important for the modelling and operation of the kiln.

The investment can only be supported if the models and the potential experimental data is used to get new guidelines for the design and operation of rotary kilns. The next chapter addresses with detail the potential further work with this respect.

Chapter 7

Further Work

From the conclusions and recommendations it can be inferred that there is much work to be done with respect to CAC Kilns. In the present chapter various areas of opportunity will be presented. Furthermore, a proposal for further work will be described.

7-1 Freeboard Model

As it was shown in the previous chapters, the one-dimensional model and the transversal two-dimensional model are dependent on data from the freeboard. Thus it is imperative to have a validated and calibrated freeboard model. This can be done with state of the art combustion models calibrated with experimental data. As it was mentioned in the previous section, a pilot kiln installation would allow to validate and calibrate such a model.

Most importantly, if one wants to use a one-dimensional model to do sensitivity analysis and to optimise the kiln design variables, one needs to develop a simplified freeboard model with low computation cost. This can be done following methodology already existing in the literature for a one-dimensional freeboard model [32] or with symmetry simplifications for a CFD model. Implicit is the fact that the simplified freeboard model must be validated and calibrated with experimental or a validated CFD 3-D model.

7-2 Chemical Reaction Kinetics and Extension of the 1-D Bed Model

In order to have a more reliable kiln model, full reaction kinetics must be developed as this would bring as a consequence a better estimation of melt fractions, heat transfer phenomena due to reactions and phase changes, and product concentration profile along the length of the kiln. This has to be done taking into account a proposal for stoichometry, XRD experimental data and information about similar reactions in the literature. This extension of the project is

adequate for Chemical Engineers or Chemists with experience in chemical reaction engineering and solids processing.

In addition to research for the development of reaction kinetics, a surface scale model must be developed taking into account the particularities of CAC production. It is imperative to develop it using experimental data from a CAC pilot kiln.

7-3 Transversal Operating Mode

As it can be observed in Chapters 1,2 and 4 the characterisation of the transversal granular flow fields is of importance as it determines to which extent the material bed is mixed in the plane normal to the axis. A DEM approach seems reasonable due to its robustness in handling dense granular flow problems [42].

However, as it was noted in the most recent ACHEMA congress[1], it is of great importance the calibration and validation with experimental data[2]. For the case of CAC Kilns, it is true due to particle non-sphericity and cohesion forces due to high temperatures.

As it is mentioned in earlier chapters, if there is a correct characterisation of the transversal flow mode of the current kiln one can identify areas of opportunity in mixing and 3-D modelling approaches. It is another reason for the investment of a pilot installation.

7-4 2-D and 3-D Models

An effect of developing a 1-D model and having a characterisation of the transversal flow is the possibility of building a 2-D and 3-D model. Such models would allow the detailed analysis of certain kiln configurations derived from the optimisation of an 1-D model. It could also hint more opportunity areas with regard to the currently operating kiln.

There are two obvious approaches for the development a 2-D/3-D kiln model: a continuum approach and a DEM approach. Both present particular advantages with regard to the analysis and design of a rotary kiln. A continuum approach can be used to follow the same methodology as with the 1-D model to vary design variables and optimise kiln design. A calibrated and validated DEM model can be used to evaluate current kiln configurations and analyse its operation to find opportunity areas. As the continuum model makes use of already developed physical correlations, its set-up is much simpler. The DEM approach on the other hand, deals with phenomena which are not yet implemented in most of the existing software. Such phenomena include radiation modelling, cohesion, sintering reactions, lining scale formation and so on.

If such models can be developed, they could be used as tools for the analysis and design of CAC kilns. One could run the 1-D model to find suitable scenarios taking account economical and technical considerations. Then one would proceed to run the more detailed 2-D/3-D models to bring further insight and start making decisions on the design of new kilns.

[1] ACHEMA, Frankfurt am Main. www.achema.de

[2] Conferences held in ACHEMA with regard to Solids Processing and DEM by: TU Hamburg-Harbourg, Institute of Solids Process Engineering and Particle Technology. Leibniz Institute for Agricultural Engineering Potsdam-Bornim. TU Berlin, Chair for Energy Process Technology and Conversion Technologies for Renewable Energies

7-5 Scale-up and Design Guidelines

The goal for the further research should not only revolve on the analysis of current CAC kilns. If one takes into account the importance of research as a way of generating knowledge, one should include in its goals the development of scale-up and design guidelines in general, noting that most of the guidelines existing in literature for rotary kilns are either obsolete or based solely in empirical considerations for Portland Cement Kilns [6].

Scale-up and design guidelines in general for rotary kilns would be an important addition for any company utilising such units. It is an area of opportunity for the funding of further research to be done described in the current chapter. In contrast, the specific knowledge to be developed for CAC Kilns would be of great value for the industrial partner and would ensure its position as a top producer in its market.

Thus it is important to add as a research goal for further work, the development of new scale-up and design guidelines for rotary kilns in order to attract funding to the prospective research. This without ignoring the fact that most of the research could lead to improvements in the design of Calcium Aluminate Kilns.

7-6 Closing Remarks

It is important to note that there is work to be done stemming out from the project presented. This opens the possibility for further involvement between university and industry. Also, by looking at the scope of the previous sections of the present work, the prospective research work requires a multidisciplinary approach to it.

The Scientific Computing group can be in charge of the implementation of complex modelling with respect with the DEM methodology and the usage of cluster computers due to its inherent expertise in this regard. However, it is to be considered the collaboration with a group with expertise in Chemical and Process Engineering. This is due to the expertise a chemical engineer has with experimental design and laboratory work, chemical reaction engineering, design and scale-up of unit operations, and plant design.

Appendix A

List of Symbols

Abbreviations

χ	Gas Layer Thickness [mm]
Ω	Form Factor [-]
α	Apsorptivity [-]
α_b	Thermal Diffusivity of Bulk Solids [-]
$\bar{\tau}$	Kiln Residence Time [s]
β	Volumetric Thermal Expansion Coefficient [-]
$\dot{m}_s$	Solids Mass Flow Rate [kg/s]
η	Kiln Load [-]
ν	Kinematic Viscosity $[m^2/s]$
ω	Angular Velocity $[s^{-1}]$
Φ	Physical Property Indication [-]
Ψ	Angle between bed surface and kiln axis [-]
ρ	Density [Kg/m^3]
σ	Stefan-Boltzmann Constant $[Wm^2K^{-4}]$
θ	Cross-sectional Half Angle [-]
ε	Emissivity [-]
ξ	Dynamic Angle of Repose [-]
A	Heat Exchange Area [m]
$c_{p,s}$	Solids Heat Capacity
D	Kiln Internal Diameter [m]
d_p	Particle Diameter [m]
D_{eq}	Equivalent Diameter [-]

e	Void Fraction [-]
E_a	Activation Energy [kJ/mol]
g	Gravity $[m/s^2]$
Gr	Grashof Number [-]
k_a	Air Thermal Conductivity [W/m K]
k_b	Thermal Conductivity of Bulk Solids $[W/mK]$
k_{eff}	Effective Thermal Conductivity [W/m K]
L_K	Total Kiln Length [m]
L_{crd}	Transversal Chord Length [m]
m_L	Melt Fraction [-]
Nu	Nusselt Number [-]
Pe	Peclet Number [-]
Pr	Prandtl Number [-]
Q	Heat Transfer Rate [W]
q	Heat Flux $[W/m^2]$
R	Kiln Radius $[m]$
Re_ω	Angular Reynolds Number [-]
Re_g	Gas Phase Reynolds Number [-]
T	Temperature [K]
U	Overall Heat transfer Coefficient
u_g	Freeboard Gas Velocity [m/s]
g,s,w	Subscripts denoting gas, solids and wall respectively

Appendix B

DEM Granular Flow Model Listing

B-1 Base Input Script File

```
variable dp equal 0.001
variable RPM equal xx
variable T_r equal 1/(${RPM}/60)
variable length equal 3*${dp}

atom_style  granular
boundary  f p f
newton    off
atom_modify sort 0 0

communicate single vel yes
units   si

region    reg cylinder y 0 0 1.05 0.0 ${length} units box
create_box  2 reg

neighbor  0.02 bin
neigh_modify  delay 0

#Material properties required for new pair styles

fix     m1 all property/global youngsModulus peratomtype 5e6 2e9
fix     m2 all property/global poissonsRatio peratomtype 0.25 0.35
fix     m3 all property/global coefficientRestitution peratomtypepair 2 &
0.35 0.1 &
0.1 1
fix     m4 all property/global coefficientFriction peratomtypepair 2 &
 0.8 0.8 &
 0.8 1
fix     m5 all property/global characteristicVelocity scalar 2.
```

```
31 fix     m6 all property/global coefficientRollingFriction peratomtypepair
       2 &
32  0.01  0.01 &
33  0.01  1
34
35 #New pair style
36 pair_style  gran/hertz/history 3 0
37 pair_coeff  * *
38
39 timestep  0.0000001
40
41 fix   1 all nve/sphere
42 fix   2 all gravity 9.81 vector 0.0 0.0 -1.0
43
44
45 #import triangular mesh from cad; the syntax is as follows:
46 fix   cad all mesh/gran cylinder3ref.stl 2 1 0. 0. 0. 0. 0. 0. rotation 0
       0 0 0 1 0 ${T_r}
47
48
49 #use the imported mesh as granular wall
50 fix   granwalls all wall/gran/hertz/history 3 0 mesh/gran 1 cad
51
52 #particle distributions
53 fix   pts1 all particletemplate/sphere 1 atom_type 1 density constant
      4000 radius constant ${dp}
54
55 fix   pts2 all particletemplate/sphere 1 atom_type 1 density constant
      4000 radius constant ${dp}
56
57 fix   pdd1 all particledistribution/discrete 1 2 pts1 .5 pts2 .5
58
59 #region of insertion
60 region    bc block -0.65 0.65 0 ${length} -1.05 -.85 units box
61
62 group   nve_group region reg
63 fix   ins nve_group insert/pack seed 56 distributiontemplate pdd1
      insert_every once overlapcheck yes volumefraction_region 0.5 region bc
64
65 fix   ts all check/timestep/gran 1000 0.1 0.1
66 compute   1 all erotate/sphere
67 thermo_style  custom step atoms ke c_1 f_ts[1] f_ts[2] vol
68 thermo    1000
69 thermo_modify lost ignore norm no
70 compute_modify  thermo_temp dynamic yes
71
72
73 #insert the first particles so that dump is not empty
74 run   1
75 dump    dmp all custom 100000 post/kiln.dump id type type x y z ix iy iz
      vx vy vz fx fy fz omegax omegay omegaz radius
76
77 dump    dumpstl all stl 100000 post/dump*.stl
```

```
78
79 #one geometry dump is enough
80 undump    dumpstl
81
82 #insert particles and settle
83 run   100000 upto
84 unfix   ins
85
86 #moving mesh
87 run     150000000 upto
```

Appendix C

1-D Granular Bed Model Code Listing

C-1 Main File

```
clear all
close all
global Dk J Lk RPM omega load Gg Ug Xi ms theta yw Twmesh Rad c Twall
    zODE Twally tau hDATA qDATA

Dk=.406;
J=500;
Lk=5.5;
RPM=1.5;
omega=RPM*pi()/30; %rad/s
load=0.12;
Q=3500;
rho_g=1.18;
%G=Q*rho_g; % Gas mass rate
G=2.05;
At=pi*(Dk/2)^2; % Transversal kiln area
Gg=G*3600/At; % Kg*m2/h
Ug=2; % Gas velocity
ms=62/3600; % Solids mass rate
Xi=pi/6;
%RESIDENCE TIME min
tau=100;

syms theta1

theta=abs(solve(load==(theta1-sin(theta1))/(2*pi)));
theta=double(theta);

T0=100+273.15;
TJ=1200;
```

```
30
31 h=Lk/J;
32 yw = linspace(0,Lk,100);
33
34 Tg=Tgas(yw);
35 Twpoly=Twpoly(yw);
36
37  M= [1 0 0 0
38      0 0 0 0
39      0 0 1 0
40      0 0 0 0];
41  options = odeset('Mass',M,'RelTol',1e-2,'AbsTol',[1e-3 1e-3 1e-3 1e-3],
        ...
42                   'Vectorized','off');
43
44 c=2;
45 zODE(1)=0;
46  [z,T]=ode15s(@dTdz1,0:h:Lk,[T0 500 .001 300]',options);
47
48 Tkg=[790 875 960 990 1000 1030 1060 1100 1120];
49 yexpg=[0.1 0.9 2.1 2.4 2.8 3.13 3.9 4.45 4.9];
50
51 Tkb=[490 650 750 810 825 850 875 940 960 1000];
52 yexpb=[0.25 0.7 1.4 2.125 2.4 2.8 3.13 3.9 4.5 4.9];
53
54 plotvalid(z,T(:,1:2),yw,Tg,yexpg,Tkg,yexpb,Tkb)
```

C-2 Validation DAE

```
1  function [ Tprime ] = dTdz1( z , T )
2  % DAE system of equations for Tshell, Tw and Ts INCLUDING RAD TSHELL
3  global J Gg ms Xi Dk omega theta Lk Ug c zODE  RPM  tau load hDATA qDATA
4
5  %%% Parameters for Lining and Shell  %%%
6  linwidth=.103;
7  steelwidth=.007;
8  klining=1.40;
9  kshell=57;
10 Tamb=20+273.15;
11 Uamb=25;
12 epssh=0.79;
13
14 %%% Parameters for Solids - Wall interface
15 shi=.096;
16
17 %%% -------------------------------- %%%
18 %%% Physical properties and composition of the solids %%%
19 Cps=740;   %Typical value from literature
20 dp=0.0025;
21
22 %%% -------------------------------- %%%
23 %%% Geometric Calculations for Area  %%%
```

```
24
25 Dz=Lk;
26 Rlin=(Dk/2)+linwidth;
27 Rshell=Rlin+steelwidth;
28 Deq=0.5*Dk*(2*pi-theta+sin(theta))/(pi-theta/2+sin(theta/2));
29
30 Aeb=2*(Dk/2)*sin(theta/2)*Dz;
31 Acw=theta*(Dk/2)*Dz;
32 Aew=2*(Dk/2)*pi*Dz-theta*(Dk/2)*Dz;
33 Ash=2*pi*(Rshell)*Dz;
34
35 %%% -------------------------------- %%%
36 %%% Dimensionless numbers            %%%
37 % For outside shell conditions
38 BetaAir=3.43; %3.43 @20C, 3.67 @0C, 3.20 @40C
39 g=9.81;
40 Reamb=Uamb*(2*Rshell)/nu_air(Tamb);
41 Rewamb=(2*Rshell)^2*omega/nu_air(Tamb);
42 Gr=g*BetaAir*(T(4)-Tamb)/(nu_air(Tamb)^2)  ;
43
44 % For freeboard conditions
45 Re=Ug*Deq/nu_air(Tg(z));
46 Pr=0.68;
47 Rew=Deq^2*omega/nu_air(Tg(z));
48
49 %%% -------------------------------- %%%
50 %%% Outer Shell heat transfer coeff and resistances %%%
51
52 if (Rewamb/sqrt(Gr)) < 0.2
53     Corr=7.4e-7; % value varied for calibration for shell losses
54     N=RPM;
55     hamb=kAir(Tamb)*PrAir(Tamb)*Corr*Reamb^N;
56 else
57     hamb=0.11*kAir(Tamb)*PrAir(Tamb)/(2*Rshell)*(Reamb^(2) + 0.5*Rewamb
           ^(2) + Gr)^.35;
58 end
59
60  sigma=5.6703e-8;
61    C1=1+((Tamb+0)/(T(4)+0))+((Tamb+0)/(T(4)+0))^2+((Tamb+0)/(T(4)+0))^3;
62    hrsa=C1*epssh*sigma*(T(4)+0)^3;
63
64 R1=(klining)/(Rlin*log((Rlin*2)/Dk));
65 R2=(kshell)/(Rshell*log(Rshell/(Rlin)));
66
67 % Resistances for Heat Transfer Paths to the shell and to ambience
68 Uamb=1/(1/R1+1/R2+1/hamb+1/hrsa);
69 Ush=1/(1/R1+1/R2);
70
71 %%% -------------------------------- %%%
72 %%% Correlations and Data for dTs/dz %%%
73 % Convective heat transfer coefficient: Gas -> Solids
74 hcgb=(kAir(Tg(z))/Deq)*0.46*Re^(0.535)*Rew^(0.104)*(load)^(-.341); %
      Mujumdar, Li
```

```
75
76 % Convective heat transfer coefficient: Gas -> Wall
77 hcgw=1.54*(kAir(Tg(z))/Deq)*Re^(0.575)*Rew^(-.292); %Mujumdar, Li
78
79 % Convective/Conductive penetration model: Solids -> Wall
80 hcwcb=(shi*dp/kAir(Tg(z))+(2*sqrt(2*kb(T(1))*rho_b*Cps*RPM/theta)^(-1)))
       ^(-1); %Li
81
82 %%% -------------------------------- %%%
83 %%% Radiation Constants %%%
84 sigma=5.6703e-8;
85 epsw=0.85;
86 epsb=0.9;
87 epsg=0.1;
88 absg=0.1;
89 OMEGA=2*(Dk/2)*sin(theta/2)/(2*(pi-Xi)*(Dk/2)); % Shape factor
90
91 %%% -------------------------------- %%%
92 %%% Heat Fluxes %%%
93 Qcgb=(hcgb*Aeb*(Tg(z)-T(1)));
94 Qcgw=hcgw*Aew*(Tg(z)-T(2));
95 Qrgb=Aeb*sigma*(epsb+1)*(epsg*(Tg(z)+0)^4-absg*(T(1)+0)^4)/2;
96 Qrgw=Aew*sigma*(epsw+1)*(epsg*(Tg(z)+0)^4-absg*(T(2)+0)^4)/2;
97 Qcwb=hcwcb*Acw*(T(2)-T(1));
98 Qrwb=sigma*Aeb*epsb*epsw*OMEGA*((T(2)+0)^4-(T(1)+0)^4);
99 Qshell=Uamb*Ash*(T(2)-(Tamb+0));
100 Qshell2=Ush*Ash*(T(4)-(Tamb+0));
101
102 %%% -------------------------------- %%%
103 % Energy Balance for the Solids
104 Tprime(1,1)= (1/(Cps*ms*Lk))*(Qcgb+Qrgb+Qrwb+Qcwb)+(1/(Cps*ms))*DHrxn;
105 % Energy Balance for the Shell/Lining (LHS=0 as this is a DAE system)
106 Tprime(2,1)=Qrgw+Qcgw-Qrwb-Qcwb-Qradamb-Qshell;
107 % Rx Kinetics *not used for validation
108 Tprime(3,1)=0;
109 % Shell energy balane
110 Tprime(4,1)=Qrgw+Qcgw-Qrwb-Qcwb-Qradamb-Qshell2;
111
112 zODE(c,:)=z;
113 hDATA(c,:)=[hcgw hcgb hcwcb Uamb];
114 qDATA(c,:)=[Qcgb Qcgw Qrgb Qrgw Qcwb Qrwb Qshell/Ash];
115 c=c+1;
116 end
```

C-3 Almatis Kiln DAE

```
1 function [ Tprime ] = dTdz1( z , T )
2 % DAE system of equations for Tshell, Tw and Ts INCLUDING RAD TSHELL
3 global J Gg ms Xi Dk omega theta Lk Ug c zODE  RPM  tau load hDATA qDATA
4
5 %%% Parameters for Lining and Shell  %%%
6 linwidth=xx;
```

```
steelwidth=xx;
klining=xx;
kshell=xx;
Tamb=20+273.15;
Uamb=25;
epssh=xx;

%%% Parameters for Solids - Wall interface
shi=xx;

%%% -------------------------------- %%%
%%% Physical properties and composition of the solids %%%
Xal2o3=xx;
Xcao=xx;
MWal2o3=101.961;
MWcao=56.0774;
rhoal2o3=3950;
rhocao=3350;

%Solid Phase Heat Capacity (Shomate Equation) CaO
Cpcao = CpCaO_s(T(1));

%Solid Phase Heat Capacity (Shomate Equation) Al2O3
Cpal2o3 = CpAl2O3_s(T(1));
rho_b=Xal2o3*rhoal2o3+Xcao*rhocao;
MWs=Xal2o3*MWal2o3+Xcao*MWcao;
Cpsmol=Xal2o3*Cpal2o3+Xcao*Cpcao; %J/mol*K
Cps=Cpsmol*1000/MWs; %J/kg*K
dp=xx;

%%% -------------------------------- %%%
%%% Geometric Calculations for Area  %%%
Dz=Lk;
Rlin=(Dk/2)+linwidth;
Rshell=Rlin+steelwidth;
Deq=0.5*Dk*(2*pi-theta+sin(theta))/(pi-theta/2+sin(theta/2));
Aeb=2*(Dk/2)*sin(theta/2)*Dz;
Acw=theta*(Dk/2)*Dz;
Aew=2*(Dk/2)*pi*Dz-theta*(Dk/2)*Dz;
Ash=2*pi*(Rshell)*Dz;

%%% -------------------------------- %%%
%%% Dimensionless numbers            %%%
% For outside shell conditions
BetaAir=3.43; %3.43 @20C, 3.67 @0C, 3.20 @40C
g=9.81;
Reamb=Uamb*(2*Rshell)/nu_air(Tamb);
Rewamb=(2*Rshell)^2*omega/nu_air(Tamb);
Gr=g*BetaAir*(T(4)-Tamb)/(nu_air(Tamb)^2)   ;
% For freeboard conditions
Re=Ug*Deq/nu_air(Tg(z));
Pr=0.68;
Rew=Deq^2*omega/nu_air(Tg(z));
```

```
60
61 %%% ------------------------------- %%%
62 %%% Outer Shell heat transfer coeff and resistances %%%
63 if (Rewamb/sqrt(Gr)) < 0.2
64     Corr=5.0e-8;  % varied to calibrate
65     N=RPM;
66     hamb=kAir(Tamb)*PrAir(Tamb)*Corr*Reamb^N;
67 else
68     hamb=0.11*kAir(Tamb)*PrAir(Tamb)/(2*Rshell)*(Reamb^(2) + 0.5*Rewamb
       ^(2) + Gr)^.35;
69 end
70  sigma=5.6703e-8;
71    C1=1+((Tamb+0)/(T(4)+0))+((Tamb+0)/(T(4)+0))^2+((Tamb+0)/(T(4)+0))^3;
72    hrsa=C1*epssh*sigma*(T(4)+0)^3;
73 R1=(klining)/(Rlin*log((Rlin*2)/Dk));
74 R2=(kshell)/(Rshell*log(Rshell/(Rlin)));
75
76 % Resistances for Heat Transfer Paths to the shell and to ambience
77 Uamb=1/(1/R1+1/R2+1/hamb+1/hrsa);
78 Ush=1/(1/R1+1/R2);
79
80 %%% ------------------------------- %%%
81 %%% Correlations and Data for dTs/dz %%%
82 % Convective heat transfer coefficient: Gas -> Solids
83 hcgb=(kAir(Tg(z))/Deq)*0.46*Re^(0.535)*Rew^(0.104)*(load)^(-.341); %
       Mujumdar, Li
84
85 % Convective heat transfer coefficient: Gas -> Wall
86 hcgw=1.54*(kAir(Tg(z))/Deq)*Re^(0.575)*Rew^(-.292); %Mujumdar, Li
87
88 % Convective/Conductive penetration model: Solids -> Wall
89 hcwcb=(shi*dp/kAir(Tg(z))+(2*sqrt(2*kb(T(1))*rho_b*Cps*RPM/theta)^(-1)))
       ^(-1); %Li
90
91 %%% ------------------------------- %%%
92 %%% Radiation Constants %%%
93 sigma=5.6703e-8;
94 epsw=0.85;
95 epsb=0.9;
96 epsg=0.1;
97 absg=0.1;
98 OMEGA=2*(Dk/2)*sin(theta/2)/(2*(pi-Xi)*(Dk/2)); % Shape factor
99
100 %%% ------------------------------- %%%
101 %%% Heat Fluxes %%%
102 Qcgb=(hcgb*Aeb*(Tg(z)-T(1)));
103 Qcgw=hcgw*Aew*(Tg(z)-T(2));
104 Qrgb=Aeb*sigma*(epsb+1)*(epsg*(Tg(z)+0)^4-absg*(T(1)+0)^4)/2;
105 Qrgw=Aew*sigma*(epsw+1)*(epsg*(Tg(z)+0)^4-absg*(T(2)+0)^4)/2;
106 Qcwb=hcwcb*Acw*(T(2)-T(1));
107 Qrwb=sigma*Aeb*epsb*epsw*OMEGA*((T(2)+0)^4-(T(1)+0)^4);
108 Qshell=Uamb*Ash*(T(2)-(Tamb+0));
109 Qshell2=Ush*Ash*(T(4)-(Tamb+0));
```

```
110
111 %%% -------------------------------- %%%
112 dtdz=tau/42;
113 %%% CONV ALUMINA (Almatis Data, simplified conversion model)
114 A=14500; %min-1
115 R=8.314;
116 Ea=205000;
117 k=A*exp(-Ea/(R*(T(1)-273)));
118 Xa0=xx;
119 T(3)=real(T(3));
120 if T(3) >= 99
121     dNdz=0;
122 else
123 dNdz=Xa0*1000*(ms/MWal2o3)*dtdz*k*D4alpha(T(3));
124 end
125 DHrxn=dNdz*30*1000;
126
127 %%%_________
128 % Energy Balance for the Solids
129 Tprime(1,1)= (1/(Cps*ms*Lk))*(Qcgb+Qrgb+Qrwb+Qcwb)+(1/(Cps*ms))*DHrxn;
130 % Energy Balance for the Shell/Lining (LHS=0 as this is a DAE system)
131 Tprime(2,1)=Qrgw+Qcgw-Qrwb-Qcwb-Qradamb-Qshell;
132 % Rx Kinetics from ME
133 Tprime(3,1)=dtdz*k*D4alpha(T(3));
134 % Shell energy balane
135 Tprime(4,1)=Qrgw+Qcgw-Qrwb-Qcwb-Qradamb-Qshell2;
136
137 zODE(c,:)=z;
138 hDATA(c,:)=[hcgw hcgb hcwcb Uamb];
139 qDATA(c,:)=[Qcgb Qcgw Qrgb Qrgw Qcwb Qrwb Qshell];
140 c=c+1;
141 end
```

Appendix D

Transversal Heat Transfer Model Code Listing

D-1 Main File: PDE Tool and Geometry

```
function pdemodel
[pde_fig,ax]=pdeinit;
pdetool('appl_cb',1);
set(ax,'DataAspectRatio',[1 1 1]);
set(ax,'PlotBoxAspectRatio',[1.5 1.5 1]);
set(ax,'XLimMode','auto');
set(ax,'YLimMode','auto');
set(ax,'XTickMode','auto');
set(ax,'YTickMode','auto');

% Geometry description:
pdeellip(0,0,1.2,1.2,...
0,'shell');
pdeellip(0,0,1.1499999999999999,1.1499999999999999,...
0,'lining');
pdeellip(0,0,1.05,1.05,...
0,'inner');
pdepoly([ -0.67635270541082138,...
 0.73647294589178403,...
 0.56212424849699438,...
 0.29759519038076165,...
 -0.1292585170340681,...
 -0.39979959919839647,...
],...
[ -0.85370741482965906,...
 -0.85370741482965906,...
 -0.9679358717434865,...
 -1.0641282565130257,...
```

```
29    -1.1002004008016031,...
30    -1.0280561122244487,...
31  ],...
32   'P1');
33  set(findobj(get(pde_fig,'Children'),'Tag','PDEEval'),'String','(shell+
        lining)-inner+P1')
34
35  % Boundary conditions:
36  pdetool('changemode',0)
37  pdetool('removeb',[3 ]);
38  pdesetbd(14,...
39  'neu',...
40  1,...
41  '0',...
42  '10000')
43  pdesetbd(13,...
44  'neu',...
45  1,...
46  '0',...
47  '10000')
48  pdesetbd(12,...
49  'neu',...
50  1,...
51  '0',...
52  '10000')
53  pdesetbd(10,...
54  'neu',...
55  1,...
56  '0',...
57  '10000')
58  pdesetbd(5,...
59  'dir',...
60  1,...
61  '1',...
62  '500')
63  pdesetbd(4,...
64  'dir',...
65  1,...
66  '1',...
67  '500')
68  pdesetbd(3,...
69  'dir',...
70  1,...
71  '1',...
72  '500')
73  pdesetbd(2,...
74  'dir',...
75  1,...
76  '1',...
77  '500')
78  pdesetbd(1,...
79  'neu',...
80  1,...
```

```
81  '0' ,...
82  '10000')
83
84  % Mesh generation:
85  setappdata(pde_fig,'Hgrad',1.3);
86  setappdata(pde_fig,'refinemethod','regular');
87  setappdata(pde_fig,'jiggle',char('on','mean',''));
88  pdetool('initmesh')
89
90  % PDE coefficients:
91  pdeseteq(1,...
92  '1.47!kb(u)!53',...
93  '0.0!0.0!0.0',...
94  '0.*(2250*800*(ux.*VxPF(x,y)+uy.*VyPF(x,y)))!0.*(ux.*rho_s.*Cp_s(u).*Vx(x
        ,y)+uy.*rho_s.*Cp_s(u).*Vy(x,y))!0.*(ux.*7850.*470.*VxPF(x,y)+uy
        .*7850.*470.*VyPF(x,y))',...
95  '1.0!1.0!1.0',...
96  '0:10',...
97  '0.0',...
98  '0.0',...
99  '[0 100]')
100 setappdata(pde_fig,'currparam',...
101 ['1.47!kb(u)!53

        ';...
102 '0.0!0.0!0.0

        ';...
103 '0.*(2250*800*(ux.*VxPF(x,y)+uy.*VyPF(x,y)))!0.*(ux.*rho_s.*Cp_s(u).*Vx(x
        ,y)+uy.*rho_s.*Cp_s(u).*Vy(x,y))!0.*(ux.*7850.*470.*VxPF(x,y)+uy
        .*7850.*470.*VyPF(x,y))';...
104 '1.0!1.0!1.0

        '])
105
106 % Solve parameters:
107 setappdata(pde_fig,'solveparam',...
108 str2mat('1','7037','10','pdeadworst',...
109 '0.5','longest','1','1e-2','1000','full','inf'))
110
111 % Plotflags and user data strings:
112 setappdata(pde_fig,'plotflags',[1 1 1 1 1 1 6 1 0 0 0 1 1 1 0 0 0 1]);
113 setappdata(pde_fig,'colstring','');
114 setappdata(pde_fig,'arrowstring','');
115 setappdata(pde_fig,'deformstring','');
116 setappdata(pde_fig,'heightstring','');
117
118 % Solve PDE:
119 pdetool('solve')
```

Bibliography

[1] ANSYS. Fluent cfd, 2012.

[2] AspenTech. Aspen plus. Process Simulator, 2012.

[3] P. Barr, J. Brimacombe, and A. Watkinson. A heat-transfer model for the rotary kiln: Part i. pilot kiln trials. *Metallurgical and Materials Transactions B*, 20:391–402, 1989. 10.1007/BF02696991.

[4] R.B. Bird, W.E. Stewart, and E.N. Lightfoot. *Transport phenomena*. Wiley International edition. J. Wiley, 2007.

[5] A.A. Boateng. Boundary layer modeling of granular flow in the transverse plane of a partially filled rotating cylinder. *International Journal of Multiphase Flow*, 24(3):499 – 521, 1998.

[6] A.A. Boateng. *Rotary kilns: transport phenomena and transport processes*. Chemical, Petrochemical & Process. Elsevier/Butterworth-Heinemann, 2008.

[7] D. Bonamy, P.-H. Chavanis, P.-P. Cortet, F. Daviaud, B. Dubrulle, and M. Renouf. Euler-like modelling of dense granular flows: application to a rotating drum. *The European Physical Journal B - Condensed Matter and Complex Systems*, 68:619–627, 2009. 10.1140/epjb/e2009-00123-6.

[8] J.K. Brimacombe and A.P. Watkinson. Heat transfer in a direct-fired rotary kiln: 1. pilot plant and experimentation. *Metallurgical Transactions*, 9B:201–208, 1978.

[9] J.K. Brimacombe and A.P. Watkinson. Heat transfer in a direct-fired rotary kiln: 2. development of the cross-section model. *Metallurgical Transactions*, 20B:403–419, 1989.

[10] CD-adapco. Star-ccm+ Reference Manual, 2012.

[11] C.T. Crowe, J.D. Schwarzkopf, M. Sommerfeld, and Y. Tsuji. *Multiphase Flows With Droplets and Particles*. Taylor and Francis, 2011.

[12] G.J. Finnie, N.P. Kruyt, M. Ye, C. Zeilstra, and J.A.M. Kuipers. Longitudinal and transverse mixing in rotary kilns: A discrete element method approach. *Chemical Engineering Science*, 60(15):4083 – 4091, 2005.

[13] H.S. Fogler. *Essentials of Chemical Reaction Engineering*. Prentice Hall International Series in the Physical and Chemical Engineering Sciences. Prentice Hall, 2010.

[14] D. Gidaspow. *Multiphase flow and fluidization: continuum and kinetic theory descriptions*. Academic Press, 1994.

[15] Isaac Goldhirsch. Introduction to granular temperature. *Powder Technology*, 182(2):130 – 136, 2008.

[16] J. Gorog, T. Adams, and J. Brimacombe. Regenerative heat transfer in rotary kilns. *Metallurgical and Materials Transactions B*, 13:153–163, 1982. 10.1007/BF02664572.

[17] H. Henein, J. Brimacombe, and A. Watkinson. Experimental study of transverse bed motion in rotary kilns. *Metallurgical and Materials Transactions B*, 14:191–205, 1983. 10.1007/BF02661016.

[18] H. Henein, J. Brimacombe, and A. Watkinson. The modeling of transverse solids motion in rotary kilns. *Metallurgical and Materials Transactions B*, 14:207–220, 1983. 10.1007/BF02661017.

[19] Michael David Heydenrych. *Modelling of Rotary Kilns*. PhD thesis, Universiteit Twente, 2001.

[20] Suketoshi Ito. Layer formation and apparent activation energies of formation of calcium aluminates. *Zeitschrift fuer Physikalische Chemie*, 1977.

[21] H. M. Jaeger and Sidney R. Nagel. Physics of the granular state. *Science*, 255(5051):1523–1531, 1992.

[22] Ursula Kääntee. Modelling a cement manufacturing process to study possible impacts of alternative fuels. *Extraction and Processing Division Meeting on Recycling and Waste Treatment in Mineral and Metal Processing: Technical and Economic Aspects*, 2002.

[23] S.J.L. Kang. *Sintering: densification, grain growth, and microstructure*. Materials science & engineering. Elsevier Butterworth-Heinemann, 2005.

[24] Ammar Khawam and Douglas R. Flanagan. Solid-state kinetic models: Basics and mathematical fundamentals. *The Journal of Physical Chemistry*, 110(35):17315–17328, 2006. PMID: 16942065.

[25] C. Kloss and C. Goniva. *LIGGGHTS: An Open Source Discrete Element Simulations of Granular Materials Based on Lammps*, pages 781–788. John Wiley & Sons, Inc., 2011.

[26] Daizō Kunii and O. Levenspiel. *Fluidization engineering*. Butterworth-Heinemann series in chemical engineering. Butterworth-Heinemann, 1991.

[27] M. Kwapinska, G. Saage, and E. Tsotsas. Mixing of particles in rotary drums: A comparison of discrete element simulations with experimental results and penetration models for thermal processes. *Powder Technology*, 161(1):69 – 78, 2006.

[28] O. Levenspiel. *Chemical reaction engineering*. Wiley, 1999.

[29] S.-Q. Li, L.-B. Ma, W. Wan, and Q. Yao. A mathematical model of heat transfer in a rotary kiln thermo-reactor. *Chemical Engineering & Technology*, 28(12):1480–1489, 2005.

[30] C. K. K. Lun, S. B. Savage, D. J. Jeffrey, and N. Chepurniy. Kinetic theories for granular flow: inelastic particles in couette flow and slightly inelastic particles in a general flowfield. *Journal of Fluid Mechanics*, 140:223–256, 1984.

[31] F. Marias. A model of a rotary kiln incinerator including processes occurring within the solid and the gaseous phases. *Computers & Chemical Engineering*, 27(6):813 – 825, 2003.

[32] E Mastorakos, A Massias, C.D Tsakiroglou, D.A Goussis, V.N Burganos, and A.C Payatakes. Cfd predictions for cement kilns including flame modelling, heat transfer and clinker chemistry. *Applied Mathematical Modelling*, 23(1):55 – 76, 1999.

[33] MATLAB. version 7.14.0 (r2012a). The MathWorks Inc., 2012.

[34] Beshir Mohamed and John H. Sharp. Kinetics and mechanism of formation of monocalcium aluminate. *J. Mater. Chem.*, 7(8), 1997.

[35] K.S. Mujumdar and V.V. Ranade. Simulation of rotary cement kilns using a one-dimensional model. *Chemical Engineering Research and Design*, 84(3):165 – 177, 2006.

[36] OpenFOAM. Open field operation and manipulation cfd toolbox documentation, 2012.

[37] A. Passalacqua and R.O. Fox. Implementation of an iterative solution procedure for multi-fluid gas - particle flow models on unstructured grids. *Powder Technology*, 213:174 – 187, 2011.

[38] R.H. Perry and D.W. Green. *Perry's chemical engineers' handbook*. Chemical Engineers Handbook. McGraw-Hill, 2008.

[39] Michele Pisaroni. Optimal combustion to counteract ring formation in rotary kilns. *CD-Adapco 2012 Users Meeting*, 2012.

[40] Luis Portela. Computational multiphase flow. TU Delft Lecture, 2012.

[41] Dennis R. Van Puyvelde. Comparison of discrete elemental modelling to experimental data regarding mixing of solids in the transverse direction of a rotating kiln. *Chemical Engineering Science*, 61(13):4462 – 4465, 2006.

[42] F. Radjai and F. Dubois. *Discrete-Element Modeling of Granular Materials*. John Wiley & Sons, 2011.

[43] K.K. Rao and P.R. Nott. *An Introduction to Granular Flow*. Cambridge Series in Chemical Engineering. Cambridge University Press, 2008.

[44] Deliang Shi, Watson L. Vargas, and J.J. McCarthy. Heat transfer in rotary kilns with interstitial gases. *Chemical Engineering Science*, 63(18):4506 – 4516, 2008.

[45] M. Syamlal. Mfix documentation: Theory guide. *Technical Note, Department of Energy*, 1993.

[46] Matthias Schumacher Uwe Küssel, Dirk Abel and Martin Weng. Modeling of rotary kilns and application to limestone calcination. *Proceedings 7th Modelica Conference, Como, Italy*, pages 20–22, 2009.

[47] Dennis R. Van Puyvelde, Michael A. Wilson, Brent R. Young, and S. James Schmidt. Modelling transverse mixing in a rolling drum. *The Canadian Journal of Chemical Engineering*, 78(4):635–642, 2000.

[48] Shijie Wang, Jidong Lu, Weijie Li, Jie Li, and Zhijuan Hu. Modeling of pulverized coal combustion in cement rotary kiln. *Energy & Fuels*, 20(6):2350–2356, 2006.

[49] K. Yamane. Steady particulate flows in a horizontal rotating cylinder. *Physics of Fluids*, 10:1419, 1998.